# BioSpec:

# A Biophysically-Based Spectral Model of Light Interaction with Human Skin

by

Aravind Krishnaswamy

A thesis

presented to the University of Waterloo

in fulfillment of the

thesis requirement for the degree of

Master of Mathematics

in

Computer Science

Waterloo, Ontario, Canada, 2005

I hereby declare that I am the sole author of this thesis. This is a true copy of the thesis, including any required final revisions, as accepted by my examiners.

I understand that my thesis may be made electronically available to the public.

# Abstract

Despite the notable progress in physically-based rendering, there is still a long way to go before we can automatically generate predictable images of biological materials. In this thesis, we address an open problem in this area, namely the spectral simulation of light interaction with human skin, and propose a novel biophysically-based model that accounts for all components of light propagation in skin tissues, namely surface reflectance, subsurface reflectance and transmittance, and the biological mechanisms of light absorption by pigments in these tissues. The model is controlled by biologically meaningful parameters, and its formulation, based on standard Monte Carlo techniques, enables its straightforward incorporation into realistic image synthesis frameworks. Besides its biophysically-based nature, the key difference between the proposed model and the existing skin models is its comprehensiveness, i.e., it computes both spectral (reflectance and transmittance) and scattering (bidirectional surface-scattering distribution function) quantities for skin specimens. In order to assess the predictability of our simulations, we evaluate their accuracy by comparing results from the model with actual skin measured data. We also present computer generated images to illustrate the flexibility of the proposed model with respect to variations in the biological input data, and its applicability not only in the predictive image synthesis of different skin tones, but also in the spectral simulation of medical conditions.

**Acknowledgements**

I would like to thank all of the people at the University of Waterloo who have helped me in various ways. First and foremost, I would like to express my immense gratitude to my advisor, Gladimir Baranoski, for his continuous words of wisdom, support and insight. He has been a constant source of motivation, and I have the deepest respect for him and his work. I would also like to thank him for showing me what makes a good researcher, for treating me with the utmost respect, and most of all for being a true friend. I would also like to thank the members of my reading committee, Jeff Orchard and Justin Wan. Their suggestions and valuable insights have been very helpful. I would also like to thank my colleagues at the Natural Phenomena Simulation Group. Michael Lam gave many helpful suggestions about the Rayleigh scattering simulations. Brad Kimmel's enthusiasm for computer graphics is always a pleasure and has been a source for many ideas. I would also like to thank Ian Bell for his encouragement, support and many discussions on spectral rendering and color.

This work would not have been possible without the support of Inscriber Technology Corporation. In particular Sue Newell and Norm Ross, who have been very accommodating and understanding as I tried to juggle school and work, as well as Chad Faragher, with whom it is always a pleasure to discuss anything related to rendering. I would like to thank Michael Anttila for being my model for the images used in the presentation of this work. I would also like to thank the many developers at Inscriber whose computers they graciously volunteered to reduce the rendering time of the images.

Finally, I would like to thank my parents and my sister Janani who have always supported and encouraged me. I would also like to thank Kim Trang for motivating me to finish this thesis, she is truly a remarkable woman.

I am also grateful for funding through the National Sciences and Engineering Council of Canada (NSERC Grant 213281) and the Canada Foundation for Innovation (CFI Project 6218).

# Table of Contents

# List of Figures

# List of Tables

# Symbols

The following symbols are used in this thesis. They are listed in order of their appearance.

| Symbol | Definition |
|---|---|
| $\lambda$ | wavelength of light |
| $\xi_i$ | a uniform random number in the interval $[0, 1]$ |
| $p$ | ray free path length |
| $r$ | radius of spheres used to represent collagen fibrils |
| $\eta_s$ | index of refraction of stratum corneum |
| $\eta_e$ | index of refraction of epidermis |
| $\eta_p$ | index of refraction of papillary dermis |
| $\eta_r$ | index of refraction of reticular dermis |
| $\eta_f$ | index of refraction of collagen fibers in the dermis |
| $\eta_m$ | index of refraction of the dermal medium |
| $F$ | Fresnel coefficient |
| $\sigma$ | aspect ratio of oblateness of stratum corneum folds |
| $\alpha$ | angle between normal of curved microarea and the normal of planar macrosurface |
| $R_{sca}$ | Rayleigh scattering amount |
| $t$ | thickness of a medium |
| $\theta$ | angle between ray direction and specimen's normal direction |
| $a_1$ | stratum corneum total absorption coefficient |
| $a_2$ | epidermis total absorption coefficient |
| $a_3$ | dermis total absorption coefficient |
| $a_{base}$ | baseline skin absorption coefficient |
| $a_{cs}$ | stratum corneum absorption coefficient |
| $a_{eu}$ | eumelanin absorption coefficient |
| $a_{ph}$ | phaeomelanin absorption coefficient |
| $a_{ce}$ | $\beta$-carotene absorption coefficient in epidermis |
| $a_{ohb}$ | oxyhemoglobin absorption coefficient |
| $a_{dhb}$ | deoxyhemoglobin absorption coefficient |

| Symbol | Definition |
|---|---|
| $a_{cd}$ | $\beta$-carotene absorption coefficient in dermis |
| $a_{bil}$ | bilirubin absorption coefficient |
| $c_{cs}$ | $\beta$-carotene concentration in stratum corneum |
| $c_{eu}$ | $\beta$-carotene concentration in eumelanin |
| $c_{ph}$ | $\beta$-carotene concentration in phaeomelanin |
| $c_{hb}$ | concentration of hemoglobin in blood |
| $c_{bil}$ | concentration of bilirubin in blood |
| $\vartheta_m$ | volume fraction of epidermis occupied by melanosomes |
| $\vartheta_p$ | volume fraction of papillary dermis occupied by whole blood |
| $\vartheta_r$ | volume fraction of reticular dermis occupied by whole blood |
| $\gamma$ | ratio of oxyhemoglobin to the total hemoglobin concentration |
| $t_s$ | thickness of the stratum corneum |
| $t_e$ | thickness of the epidermis |
| $t_p$ | thickness of the papillary dermis |
| $t_r$ | thickness of the reticular dermis |
| $R_{att}$ | attenuation cross section |
| $R_{abs}$ | absorption cross section |
| $R_{sca}$ | scattering cross section |
| $k$ | wave number (propagation constant in vacuum) $k = \frac{2\pi}{\lambda}$ |
| $\alpha$ | polarizability |
| $\varrho(i\alpha)$ | complex portion of index of refraction of particle describing permeability |
| $p(\cos\theta)$ | probability of light being scattered in the direction given by the outgoing angle $\theta$ |
| $I$ | intensity of scattered light |
| $I_o$ | intensity of incident light |
| $\Theta$ | scattering angle |
| $d$ | distance to the center of the particle |
| $m$ | complex refractive index of the particle (=$\infty$ for totally reflecting spheres) |
| $r$ | radius of the particle |
| $N$ | number of particles in the volume |
| $\eta$ | real refractive index of the particle |
| $\delta$ | anisotropic factor of 0.035 to account for varying index of refraction |
| $V_s$ | volume of the sphere $\left(\frac{4}{3}\pi r^3\right)$ |

# Chapter 1

# Introduction

The modeling of light interaction with human skin is relevant in a variety of fields such as medicine, the cosmetics industry and realistic image synthesis. By studying processes involved in light remission from skin through computer simulations, better protocols can be developed to automatically diagnose medical conditions, such as jaundice (yellowish hue) [70], erythema (redness) [61], as well as tumors at early stages [13]. Understanding how light is absorbed and propagated in skin tissues can assist in the design of lotions protective against harmful solar radiation, and also in the design of superior cosmetics. The games and entertainment industries can also certainly benefit from being able to automatically generate realistic and predictable images of skin tissues. Creating believable images of human beings is usually an art left entirely to designers and animators. Artists currently model skin by carefully adjusting rendering parameters such as textures and colors. Despite its importance, the predictive rendering of organic materials, such as human skin, is still in its infancy, and many issues remain unsolved [68].

The predictive simulation of both the spectral and the spatial distribution of the light incident on human skin is still an open problem not only in computer graphics, but also in biomedicine and colorimetry. In this thesis, we address this issue by proposing an algorithmic biophysically-based spectral model (henceforth referred to as BioSpec) specifically designed to account for the biological factors that affect light propagation and absorption in skin tissues. The BioSpec model is function-

ally comprehensive, *i.e.*, it takes as input, biological and structural data and provides as output both spectral and scattering data for skin specimens. The former are provided in terms of reflectance and transmittance values, while the later are given in terms of BSSDF (bidirectional surface-scattering distribution function), which can be decomposed into the BRDF (bidirectional reflectance distribution function) and BTDF (bidirectional transmittance distribution function) components. The proposed model is controlled by biologically meaningful parameters determined through experiments described in the scientific literature, and its implementation, based on standard Monte Carlo Methods, enables its straightforward incorporation into most rendering frameworks. The spectral and scattering quantities can be either computed and used on the fly during the rendering process or stored in a database to be used off-line.

The remainder of this thesis is organized as follows. The next chapter describes the skin tissues and how they absorb and scatter light. Chapter 3 presents previous work from the areas of biomedicine and computer graphics. Chapter 4 presents the algorithmic BioSpec model. Chapter 5 describes the approach used to evaluate the proposed model and presents the results from the model. Chapter 6 concludes the thesis and outlines directions for future work.

# Chapter 2

# Biological Aspects of Human Skin

Skin is a multilayered and inhomogeneous organ (Figure 2.1). In this chapter, we outline the biological characteristics of its main constituents, and how they affect the propagation and absorption of light. We first present a structural overview with a description of the spectral properties of human skin. We then discuss the scattering profile of human skin.

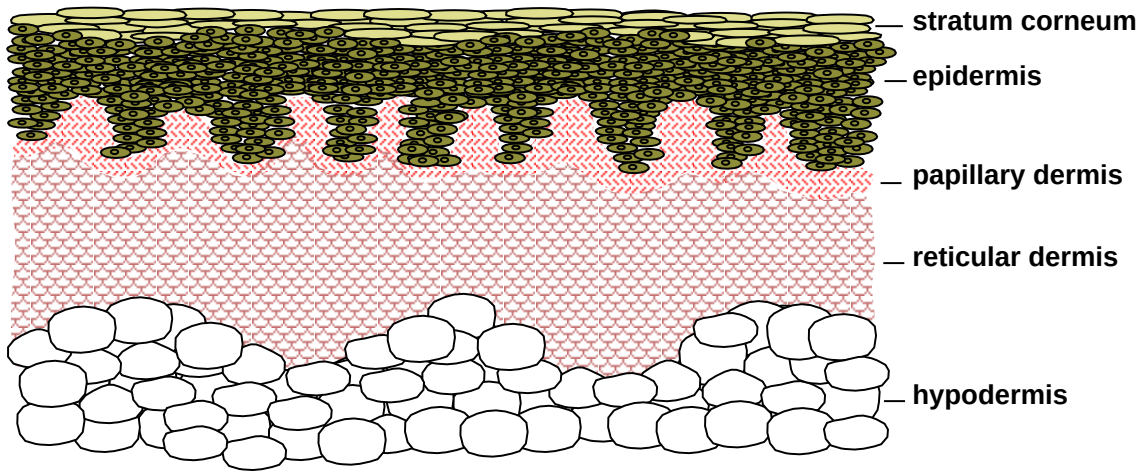


Figure 2.1: *Schematic cross-section of human skin tissues and the subcutaneous fat tissue (hypodermis).*

## 2.1 Structural Overview and Spectral Properties

The first and outermost section of human skin is the stratum corneum, which is a stratified structure approximately 0.01-0.02 $mm$ thick [3, 52]. There are skin structural models, however, that consider it part of another tissue, namely the epidermis [88] (Figure 2.1). The stratum corneum is composed mainly of dead cells, called corneocytes, embedded in a particular lipid matrix [82]. Light absorption is low in this tissue, with the amount of transmitted light being relatively uniform in the visible region of the light spectrum [20].

The epidermis is a 0.027-0.15$mm$ thick structure [3, 17, 52] composed of four layers (stratum basale, stratum spinosum, stratum ganulosum and stratum lucidum). The epidermis propagates and absorbs light. The absorption property comes mostly from a natural chromophore, melanin. There are two types of melanin, the red/yellow phaeomelanin and a brown/black eumelanin [84]. Their extinction* spectra are broad (Figure 2.2), with higher values for shorter wavelengths. The skin color is mostly associated with the eumelanin [84]. The ratio between the concentration of phaeomelanin and eumelanin present in human skin varies from individual to individual, with much overlap between skin types [84]. Recent studies reported values between 0.049 and 0.36 [63]. Melanin is produced by cells called melanocytes occurring in the stratum basale, and it is found in membranous particles called melanosomes. The melanin absorption level depends on how many melanosomes per unit volume are in the epidermis. Typically, the volume fraction of the epidermis occupied by melanosomes varies from 1.3% (lightly pigmented specimens) to 43% (darkly pigmented specimens) [36].

The dermis is a 0.6-3$mm$ thick structure [3, 17, 52] which also propagates and absorbs light. It can be divided into two layers: the papillary dermis and the reticular dermis (Figure 2.1). These layers are primarily composed of dense, irregular connective tissue with nerves and blood vessels (smaller ones in the papillary, and larger ones in the reticular dermis). The volume fraction of blood in tissue can vary, roughly in the 0.2-7% range [22, 36]. The fluence rate of blood decreases as

*The extinction coefficient of a pigment present in a tissue can be obtained by multiplying its spectral molar extinction coefficient by its estimated concentration in the tissue. [33]

we get deeper into the skin, following an almost linear pattern in the dermis [93]. In the blood cells we find another natural chromophore, hemoglobin, which absorbs light and gives blood its reddish color. Normally, the hemoglobin concentration in whole blood is between 134 and $173 g/L$ [101]. In the arteries, 90-95% of hemoglobin is oxygenated, and in the veins, more than 47% of the hemoglobin is oxygenated [4]. These two types of hemoglobin, namely oxygenated and deoxygenated hemoglobin, have slightly different extinction spectra (Figure 2.2). Two other blood borne pigments are found in the dermis, bilirubin and $\beta$-carotene, which contribute to the yellowish or olive tint of human skin (Figure 2.2). We remark that $\beta$-carotene may be also found in the epidermis and stratum corneum [1, 45].

The hypodermis is a subcutaneous adipose tissue characterized by a negligible absorption of light in the visible region of the spectrum [22]. It is usually not considered part of the skin, and its size varies considerably throughout the body. It can be up to $3cm$ thick in the abdomen and absent in the eye lids. The hypodermis presents significant deposits of white fat, whose cells are grouped together forming clusters. Due to the presence of these white fat deposits, most of the visible light that reaches this tissue is reflected back to the upper layers [17].

## 2.2 Scattering Profile

The scattering profile of human skin has two main components: surface and subsurface scattering. Surface scattering follows Fresnel equations [81], and it is affected by the presence of folds in the stratum corneum. The aspect ratio of these mesostructures depends on biological factors such as aging and hydration [82, 83]. Approximately 5-7% of the light incident (over the entire spectrum) on the stratum corneum is reflected back to the environment [88]. The remaining portion is transmitted to the internal tissues. Besides the reflective-refractive scattering caused by the reflection and refraction of light at cellular boundaries, two other types of subsurface scattering occur within the skin layers: Mie and Rayleigh scattering [36].

The stratum corneum and the epidermis are characterized as forward scattering media [7]. In

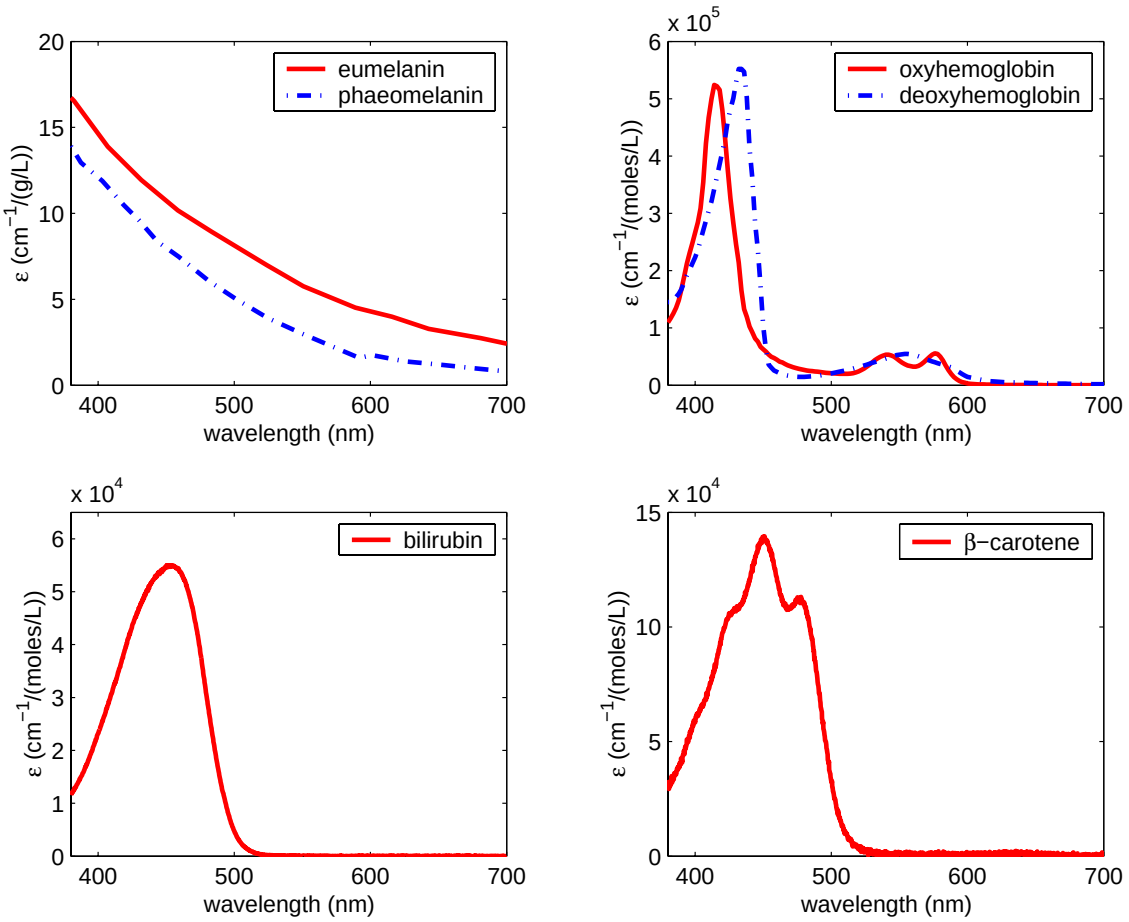


Figure 2.2: *Spectral molar extinction coefficient curves for the natural pigments present in skin tissues. Courtesy of S. Prahl and the Oregon Medical Laser Center (OMLC).*

the former this behavior is due to the alignment of the fibers, while in the later it is due to Mie scattering caused by particles that are approximately the same size of the wavelength of light (*e.g.*, cell organelles). The level of forward scattering for these tissues is wavelength dependent. Bruls and Leun [7] performed goniometric experiments for five wavelengths for both the stratum corneum and the epidermis, and they showed that the scattering profiles are broader towards the shorter wavelengths.

In the dermis, collagen fibers (approximately $2.8\mu m$ in diameter and cylindrical [36]) are responsible for Mie scattering, while smaller scale collagen fibers and other micro-structures are re-

sponsible for Rayleigh scattering [36]. Light gets scattered multiple times inside the dermis before it is either propagated to another layer or absorbed. This means that the spatial distribution of the light scattered within the dermis quickly becomes diffuse [3]. In fact, Jacques *et al.*, [37] showed through goniophotometric measurements that backscattered light from the dermis is diffuse. While Mie scattering produces variations on both ends of the visible region of the light spectrum, Rayleigh scattering, being inversely proportional to the wavelength of light ($\approx \lambda^{-4}$), produces larger variations on the low end of the light spectrum [36, 27].

# Chapter 3

# Previous Work

There is a considerable amount of research on skin optics available in the medical and biomedical literatures [88], as well as recent investigations in pattern recognition [57] and colorimetry [17]. The modeling approaches used in these areas can be loosely classified into deterministic (*e.g.*, applying Kulbelka-Munk, diffusion theories [3, 13, 14, 16, 17, 93], and radiative transfer theory [67, 90]) and nondeterministic (*e.g.*, applying Monte-Carlo methods [93, 12, 23, 52, 53, 57, 65, 66, 74, 75, 86, 99, 100, 105]). There are also skin color manipulation techniques based on image processing algorithms [87, 29, 55, 58, 61]. However, since these techniques rely on the existence of a skin simulation model (*i.e.* these techniques do not discuss the model itself), they should be examined outside a modeling context. In this chapter, we examine relevant modeling approaches used in the biomedical field as well as related work available in the computer graphics literature.

## 3.1 Light Interaction with Human Skin in Biomedicine

In biomedicine, models are mostly aimed at the reproduction of skin spectral properties to determine the content and distribution of various substances [86, 106], *i.e.*, scattering properties affecting skin appearance are usually not addressed. Moreover, a substantial portion of the work done by the biomedical community is either laser-based or aimed at wavelengths outside the visible region of

the light spectrum. The work in the biomedical community can be subdivided into four categories: Kubelka-Munk Theory based models, Diffusion Theory based models, Radiative Transfer models and Monte Carlo based models.

### 3.1.1 Kubelka-Munk Theory Based Models

Kubelka and Munk [44] developed a simple relationship between the scattering and absorption coefficients* of layers of paint and its overall reflectance. This relationship, known as Kubelka-Munk theory (K-M), applies energy transport equations to describe the radiation transfer in diffuse scattering media. Two parameters are used in the description: scattering and the absorption coefficients. The K-M theory, as originally stated, is considered to be a two-flux theory, since only two types of diffuse radiant flux are involved: a diffuse downward flux and a diffuse upward flux. The relationship between the fluxes are expressed by two simultaneous linear differential equations [44]. The original K-M theory also assumes that the medium presents inhomogeneities which are small compared to its thickness.

The K-M theory based models (henceforth referred to as K-M models), used in tissue optics, also called flux models [11], use K-M equations relating tissue optical properties to measured reflectance and transmittance. Although they are based on the two-flux K-M theory, these models expanded the original K-M formulation by adding more coefficients and/or fluxes. For example, van Gemert and Star [94] included a phase function†, effective optical depth‡ and the effective albedo§ in their K-M model. They used a phase function consisting of a combination of a forward peaked and a symmetric scattering to represent the tissue's expected experimental scattering behavior. Tuchin *et al.* [89, 102] used a four-flux model composed of the two diffuse fluxes used in the original K-M theory,

*The absorption and scattering coefficients represent the product of the actual absorption (or scattering) cross section by the density of the absorbers (or scatterers) [34]. The absorption and scattering cross sections of a particle have the dimension of area, and, generally, they are functions of the orientation of the particle and the state of polarization of the incident light [92].

†A phase function represents the directional scattering of the light incident onto a particle [92].

‡The effective optical depth represents the ratio of transmitted intensity to incident intensity multiplied by the total attenuation coefficient [94]. The term 'effective' used in this context refers to the tissue as a whole.

§The effective albedo represents the ratio between the scattering coefficient and the total attenuation coefficient, which is given by the sum of the absorption coefficient and the scattering coefficient [34].

and two collimated laser beams, the incident one and the one reflected from the bottom boundary of the specimen. Yoon *et al.* [105, 103] used a seven flux model to obtain a three dimensional representation of the scattered radiation caused by an incident laser beam in a semi-infinite medium (infinite in x and y, but finite in z).

In skin optics, the K-M theory was initially applied to specific skin tissues. Anderson and Parish [3] used a K-M model to compute absorption and scattering coefficients for the dermis tissues. Wan *et al.* [97] extended this model to compute the absorption and scattering coefficients for the epidermis tissues, taking into account both collimated and diffuse incident irradiance. In both cases [3, 97], the forward scattering in the epidermis was not considered. Diffey [16] proposed a K-M model which added two features to the previous models. It takes into account forward and backward scattering and allows changes in the refractive index at the air/skin interfaces. Cotton and Claridge [14] proposed a model to determine the color of human skin which applies the K-M equations to the dermis layer. This model takes into account the presence of melanin and blood pigments. Recently, Doi and Tominaga presented a model which considers the skin composed of two layers: epidermis and dermis. They apply the K-M theory to both layers. Their model provides weights for five skin pigments (melanin, carotene, oxy-hemoglobin, deoxy-hemoglobin and bilirubin) as well as the skin surface reflectance. These six parameters are obtained by fitting the estimated reflectance to measured values using the least squares method [8].

Although the K-M theory allows a simple quantitative treatment of skin spectral properties and recent extensions to the original two-flux theory have improved its applicability to biological tissue optics, it is not a thorough model of optical radiation transfer. The K-M models can be considered analytical, and they allow the rapid determination of skin optical parameters through inversion procedures*. However, the relative simplicity and speed of these models are achieved at the expense of accuracy [88], which requires a more detailed analysis of the structure and optical properties of the different skin tissues.

*An inversion procedure is a way to derive biochemical and optical properties from *in situ* and non-destructive experiments [24]. "Inversion" implies a reversal of the usual process of calculating reflection and transmission, *i.e.*, reflectance and/or transmittance values are used as input instead of output.

### 3.1.2 Diffusion Theory Based Models

Photon propagation in optically turbid media, such as skin tissues, can be described using the Boltzmann photon transport equation[34], which requires the optical properties to be described in terms of the scattering coefficient, the absorption coefficient and a phase function. An approximation of this equation, called diffusion approximation combines the scattering coefficient and the phase function into one parameter called the reduced scattering coefficient.

Models based on the diffusion approximation[95] or combined with other approaches, such as the K-M theory [94, 93] or Monte Carlo methods [98], have been used in biomedical investigations involving light propagation in turbid media. Farrell and Patterson [21] proposed a model based on the diffusion theory to be used in the non-invasive determination of the absorption and scattering properties of mammalian tissues. Their model incorporates a photon dipole source [25, 32] in order to satisfy the tissue boundary conditions. Recently, Doornbos *et al.* [18] proposed a method based on the diffusion theory for measuring optical properties *in vivo* and deriving chromophore concentrations from diffuse reflection measurements at the surface of skin. Section 3.2.3 contains a further discussion of this technique and its application in a computer graphics model.

Models based on diffusion approximation are relatively easy to use, place minor constraints on the geometry of the sample and can be resolved analytically [67]. The diffusion approximation, however, can be applied only when scattering events are significantly more probable than absorption events. This is usually the case for mammalian tissues in the red and near infrared regions of the light spectrum[23], thus, diffusion models have been used in medical applications involving red lasers [95, 104]. When the absorption coefficient of a turbid medium is not significantly smaller than the scattering coefficient, the diffusion theory provides a poor approximation for the photon transport equation [67, 73, 104].

### 3.1.3 Radiative Transfer models

The K-M and diffusion theories mentioned in the previous sections can be seen as special cases of the radiative transfer phenomena. When non-stochastic accurate solutions of the radiative transport

equation in biological tissues are required, more robust methods need to be used, *e.g.*, the successive scattering technique, Ambartsumian's method, the discrete ordinate method, Chandrasekhar's X and Y functions and the adding-doubling method [65]. Their applicability, however, is usually limited to simple conditions and slab geometries*. A comprehensive review of these methods is beyond the scope of this work, and the interested reader is referred to the texts by van de Hulst [90] and Prahl [65]. It is, however, worth noting that the adding-doubling method has several advantages with respect to the other techniques. It permits asymmetric scattering, arbitrarily thick samples, Fresnel boundary conditions, and relatively fast computation [65]. The adding method requires that the reflection and transmission of two slabs be known. They are used to compute the reflection and transmission of another slab comprised of these two individual slabs. In its original definition, the doubling method corresponds to the special case in which both slabs are identical [90]. Later on, it was extended to include the addition of two non-identical slabs [65]. Once the transmission and reflection for a thin slab are known, the reflection and transmission for a target slab can be computed by doubling the thickness of the thin slab until it matches the thickness of the target slab.

Prahl *et al.* [67] applied an inverse adding-doubling method (IAD: "inverse" implying its use as an inversion procedure) to determine the scattering, absorption coefficient and the asymmetry factor† of biological tissues. The IAD is an iterative method which consists of guessing a set of optical properties, calculating the reflection and transmission using adding-doubling method, comparing the calculated values with the measured reflection and transmission, and repeating the process until a match is obtained. This method may be used when the propagation of light through the specimen can be described by the one-dimensional radiative transport equation. The accuracy of this method, however, depends on the criteria applied to define a "sufficiently thin slab" [65]. There are also restrictions on the sample geometry, *i.e.* it must be a uniformly illuminated and homogeneous slab [67].

*In the tissue optics context, a "slab" refers to an infinite plane parallel layer of finite thickness [65].

†The asymmetry factor correspond to the mean cosine of the scattering angles [92]. It also corresponds to the asymmetry parameter of phase functions.

### 3.1.4 Monte Carlo Based Models

The Monte Carlo method was originally proposed by Metropolis and Ulam [54] to simulate radiative transfer which was accomplished by a stochastic model keeping track of photon trajectories. Since then, many simulation problems have been tackled using Monte Carlo techniques, including the transport of light in tissue [65]. The essence of the Monte Carlo approach is to launch a photon at an interface, and once launched, the photon is continually propagated and scattering until it is either absorbed by the tissue or escapes from the tissue from some boundary.

There are two methods in which to perform this process. The first, called fixed stepsize, evaluates whether a photon is absorbed, scattered or propagated with no interaction at fixed intervals through the medium. Prahl [65] suggests one-tenth of a mean free path* as a good stepsize. At each step in the evaluation, the events of absorption and scattered are assumed to be independent and thus only one such event can occur. The second method, called variable stepsize, forces a photon to be either absorbed or scattered at each interaction.

Simulation of absorption due to a chromophore can be performed using Beer's law or its variations. The simulation of scattering can be performed using a phase function. One such phase function is the Henyey-Greenstein Phase Function (HGPF), and to the best of our knowledge its use for the simulation of tissue was first proposed by Prahl in 1988 [65]. However, the suitability of using the HGPF in the simulation of biological tissue has started to be questioned [5, 56]. It is also worth noting that the HGPF was designed to fit observations on the radiation of galaxies and is not based on any mechanistic theory of scattering. Furthermore, it has no biological basis.

Monte Carlo models have been used extensively in the simulation of biological tissues. The models are easy to implement and provide rigorous solutions for even complex tissues. Since Monte Carlo methods converge to a solution within some acceptable error definition, theoretically, any level of accuracy can be achieved [65]. However, in practice, the accuracy of a model is limited by the accuracy and validity of the input parameters as well as the mechanisms for accounting for scattering and absorption. To the best of our knowledge, Monte Carlo models in biomedicine

*The mean free path is the average distance a photon will travel before it is either scattered or absorbed. [65]

[12, 52, 53, 66, 74, 75], colorimetry [86] and pattern recognition [57] provide only reflectance and transmittance readings for skin samples, *i.e.*, BRDF and BTDF quantities for the whole skin are not computed. Furthermore, these models are mostly aimed at laser applications, and comparisons of modeled reflectance and transmittance values with actual measured values are scarce.

## 3.2 Light Interaction with Human Skin in Computer Graphics

In computer graphics, the focus has been on developing scattering models to be incorporated into image synthesis frameworks. Although the application requirements are somewhat different, algorithms and techniques used in the models mentioned in the previous section have been incorporated in computer graphics. In this section we describe the most relevant models developed by the computer graphics community to render human skin. We present an overview as well strengths and limitations of each of these models, which include the multiple-layer scattering model [30], the discrete-ordinate model [76] and the diffusion theory based model [39].

### 3.2.1 Multiple-layer Scattering Model

#### Overview

Hanrahan and Krueger [30] presented a model for simulating the reflection of light from layered surfaces. This model henceforth referred to as H-K model has been applied in a variety of areas for the simulation of various materials such as leaves, skin, snow and paint. However, in this thesis the H-K model is examined only in the context of rendering human skin. Ng and Li [59] later extended the H-K model to include an outer layer of oil and sweat called sebum.

Subsurface scattering within the H-K model is derived using one-dimensional linear transport theory, which is a heuristic description and is a simplification of the more general volume rendering equation. The materials themselves are described as a macroscopic average of the underlying microscopic material properties. They assume a planar surface and use Fresnel equations to compute the radiance reflected and transmitted across the planar boundary. They derive an analytic first order

approximation for the amount of backscattered radiance based on Chandrasekhar's analytic solution to the integral equation. Using this expression, they can simulate single order subsurface scattering across the various layers. However, they claim deriving analytic solutions for multiple scattering quickly becomes intractable, hence they resort to a Monte Carlo algorithm for multiple scattering. We remark the multiple scattering algorithm used by the H-K model was originally proposed by Prahl [66] to study laser irradiation in tissue.

Each layer in the H-K model has five input parameters: the index of refraction, the thickness of the layer, the absorption coefficient, the scattering coefficient and the mean cosine of the phase function. The Henyey-Greenstein phase function (HGPF) was the phase function of choice. Human skin was modelled as two layers, namely the epidermis and the dermis.

#### Strengths and Limitations

The H-K model has the distinction of being the first model in computer graphics to simulate the interaction of light with organic materials using a physically plausible approach. The goal of the H-K model was to simulate a large class of materials with subsurface scattering properties. This generality means the model overlooks properties that are specific to human skin, such as the absorption of light by natural pigments. In order to visualize these spectral characteristics of human skin, the user is required to enter the tissues' absorption coefficients. These coefficients can come from biomedical literature which in turn are derived using inversion techniques. In addition, the H-K model does not provide reflectance and transmittance values, hence it is a scattering model only.

In the H-K model, the Torrance-Sparrow model is used to simulate a thin layer of oil on the outer surface that reflects light. However, there is no underlying biological justification for the use of the Torrance-Sparrow model. In addition, the parameters to the Torrance-Sparrow model are not biologically meaningful as it was developed to model the interaction of light with inorganic materials. The use of the HGPF is also of concern. The parameter 'g' (the mean cosine of the phase function, i.e., its asymmetry factor) in the HGPF has no biophysical meaning and is abstract. Also, *Baranoski et al.*[5] have recently demonstrated that the use of the HGPF for the simulation of

scattering in human skin tissue may lead to incorrect results.

The H-K model was evaluated solely through visual inspection. Several images are shown to demonstrate the effects of the Fresnel factor as well Seeliger's Law *. In addition a final image was rendered with texture maps and color data entered manually. There is no comparison of the model with actual BRDF data. This lack of comparison makes it difficult to validate the model in any meaningful way, making its predictability difficult to determine.

### 3.2.2 Discrete-Ordinate Model

#### Overview

The Discrete-Ordinate Model, henceforth referred to as the D-O model was presented by Stam [76] for simulating the interaction of light with a layer bounded by two rough surfaces. The model is a discrete ordinate approximation of radiative transfer, and it is based on the work of Stamnes and Conklin [77]. The discrete ordinate method divides the radiative transport equation into *n* discrete fluxes to obtain *n* equations with *n* unknowns. The equations are then solved numerically using Fourier transforms and eigenanalysis, an approach inspired by Jin and Stammes [40].

The discrete equations for the BRDF and BTDF are then used to generate a large dataset for the different values of the parameters. This dataset is then compressed by the use of cosine lobes, whose terms were chosen by visual inspection. The data is further compressed by fitting them to a cubic Bèzier surface. The control points of the Bèzier surface were constrained such as to obey the reciprocity rule†.

The parameters to the D-O model are the albedo and the asymmetry factor of the phase function. The HGPF was chosen as the phase function. There is also an additional parameter to represent the roughness of the surfaces that bound the skin layer. All of these parameters are dimensionless.

*Seeliger's Law represents a special case for backscattered radiance that ignores Fresnel effects and expresses it as the product of incident radiance with the ratio of the cosine of the incident angle and the sum of the cosines of the incident and reflected angles. [30]

†Reciprocity states that if we reverse the roles of incident and reflected energy, the results are the same, *i.e.*, nothing happens. [27]

#### Strengths and Limitations

The D-O model does not provide reflectance or transmittance results, hence it is also only a scattering model. The input parameters are also not biologically motivated and the model does not take into account biological process or structural details of human skin. In addition, the simplification of the biological processes within the model are not accompanied by the mathematical complexity of the algorithms. In fact, Monte Carlo algorithms offer much more simplicity. One of the advantages of the D-O model over Monte Carlo models is its speed. However, the increase in speed is achieved through precomputation and compression of generated data. We remark that similar techniques can be used with data generated by Monte Carlo algorithms to improve their speed.

The use of the HGPF is also suspect as mentioned earlier. The D-O model also lacks experimental validation and, therefore, its predictability cannot be determined. The results of the model are visually compared against a Lambertian shader and the H-K model. There are noticeable differences between the images generated by the D-O model and the Lambertian shader. However such differences are not as pronounced as one may expect from a model whose formulation has a degree of complexity few orders of magnitude higher than the well known Lambertian model.

### 3.2.3 Diffusion Theory based Model

#### Overview

Jensen *et al.* [39] proposed a model for simulating the appearance of subsurface light transport in diffusive materials in which the scattering simulation algorithm was based on the diffusion theory (Section 3.1.2). In their model, henceforth referred to as D-T model, the general concept of the BSSRDF (bidirectional scattering-surface reflectance distribution function) [60] was used to describe the transport of light from one point on a surface to another. The performance of the D-T model was later improved by introducing a two-pass hierarchical algorithm [38].

Based on their observations, Jensen *et al.* [39] theorized that due to the effects of repeated multiple scattering, the light distribution tends to become symmetric (equal in all directions) and

blurred in highly scattering media. Since the diffusion theory does not have a general analytical solution for finite media, they modeled subsurface reflection as a semi-infinite medium. They used a diffusion approximation for isotropic media called the dipole method proposed by Fretterd *et al.* [25] and Hirko *et al.* [32] and further developed by Eason [19] and Farrell *et al.* [21]. In the dipole method, two point sources are placed relative to the surface, one the positive real light located below the surface and the other a negative virtual light positioned above the surface. Using this method, they computed an analytical expression for the radiant exitance at some point from the incident flux at another point. It is important to note that Jensen *et al.* propose the use of the analytic expression for single scattering as presented by Hanrahan and Krueger. They suggest the use of this diffusion approximation in place of Monte Carlo simulation for computing multiple scattering.

The D-T model has four input parameters: the absorption coefficient, the reduced scattering coefficient, the diffuse reflectance and the index of refraction. In order to determine the values of these parameters for various materials, they used a 3-CCD video camera to observe the radiant exitance across the surface of the material. They then used diffusion theory to compute the absorption coefficient and reduced scattering coefficient. In their follow-up work, Jensen *et al.* [38] reduce the space of parameters of the D-T model to the diffuse reflectance and an average scattering distance. It is also important to note that the follow-up work presents a more efficient scheme for sampling the incident flux due to subsurface scattering and does not alter the fundamentals or equations of the original work.

#### Strengths and Limitations

The usual assumption made in tissue optics that light entering a material leaves the material at the same position is relaxed in the D-T model. From a theoretical point of view, this is a valid contribution since such an assumption fails to represent the real behavior of diffusive or translucent materials. In practice, however, the effects of this assumption on the actual appearance of the materials may not be as significant as the effects resulting from other assumptions such as the homogeneity of the materials.

The D-T model is relatively simple to implement, general (can be used for different diffusive materials), and it is not as computationally expensive as Monte Carlo based models. In addition, it can be used to render visually pleasing images. These reasons may have motivated its incorporation (or some variant) in commercial rendering packages. However, similarly to the H-K model, it presents some limitations associated to its generality. It does not take into account properties specific to organic materials. Also, like the H-K model, the input parameters come either from inversion procedures or can be arbitrarily set by the user (in the case of the simplified set of parameters [38]). Due to the fact that spectral properties such as the diffuse reflectance are actually input parameters to the model, it shall be classified only as a scattering model.

The D-T model considers the entire skin structure as one medium. As described in Chapter 2, skin is heterogeneous and layered, with each of the layers having different biological and optical properties (particularly the epidermis and dermis). It is reasonable to assume that diffusion approximation can be applied to simulating subsurface scattering in the dermis [95], however, there are some issues regarding its use for other skin layers. First, the diffusion approximation is not suitable when the scattering is mostly in the forward direction [23, 26, 104]. As mentioned in Chapter 2, the measurements performed by Bruls and van der Leun [7] demonstrate that both the stratum corneum and the epidermis tissues are highly forward scattering media. Second, as mentioned in Section 3.1.2, the diffusion theory is not applicable when the absorption coefficient is not significantly smaller than the scattering coefficient for turbid media [73, 78, 104]. Recall that human skin is characterized by the presence of pigments, such as melanin particles, which have a significant absorption cross section [10]. This issue is particularly a problem for heavily pigmented specimens.

The evaluation of the D-T model and its variant is also based solely on visual inspection. There is no comparison to actual BRDF and BTDF values of any organic (or inorganic) material. An image of a human face was generated using the model to illustrate its suitability to render believable images. We remark that the model input parameters were obtained using an inversion procedure based on the use of video camera and diffusion theory. The image was compared to an image rendered using a simple Lambertian BRDF model. As expected, differences are noticeable.

### 3.2.4 Summary

Although the computer graphics skin models are biologically motivated, they do not simulate important biological processes, such as the absorption of light by natural chromophores (pigments), which are closely tied with skin spectral properties. As a result, they must rely on spectral parameters (*e.g.*, reflectance and transmittance) either set by the user or obtained in the literature, which are specimen specific and limited to a narrow range of illuminating and viewing geometries. It is important to note that there are also several other subsurface scattering models in the graphics literature which are either not biologically motivated or specifically designed to simulate other organic materials (*e.g.*, plants [6] and hair [49]).

# Chapter 4

# BioSpec Description

In this chapter, we present the biophysically-based spectral model, henceforth referred to as BioSpec. An overview of the model is followed by a summary of its input data and parameters, and a detailed description of the scattering and absorption simulation processes.

## 4.1 Overview

BioSpec has four important defining characteristics:

1. its parameters are biophysically-meaningful,
2. it simulates and accounts for the spectral aspects of the visual appearance of human skin (reflectance and transmittance),
3. it simulates and accounts for the spatial aspects of the visual appearance of human skin (BRDF and BRDF), and
4. it simulates the subsurface scattering properties of human skin.

In the BioSpec model, light propagation is described in terms of ray optics, and the wavelength of light ($\lambda$), a physical optics [27] parameter, is included by associating a wavelength with each ray.

The propagation of light in the skin tissues is simulated as a random walk process [6], whose states are associated with the following interfaces:

1. air $\Leftrightarrow$ stratum corneum;
2. stratum corneum $\Leftrightarrow$ epidermis;
3. epidermis $\Leftrightarrow$ papillary dermis;
4. papillary dermis $\Leftrightarrow$ reticular dermis;
5. reticular dermis $\Leftrightarrow$ hypodermis.

Once a ray hits the skin specimen at interface 1, it can be reflected back or refracted into the stratum corneum. From there, the ray can be reflected and refracted multiple times within the skin layers before it is either absorbed or propagated back to the environment through interface 1. Recall that the subcutaneous tissue is a highly reflective medium (Section 2). Hence, for body areas characterized by the presence of hypodermis, it is assumed total reflection at interface 5.

In the random walk implemented by the BioSpec model, the transition probabilities are associated with the Fresnel coefficients [6] computed at each interface (assuming that the cells are locally flat, *i.e.*, they are large with respect to the wavelength of the incoming light), and the termination probabilities are associated with the free path length ($p$) computed when a ray travels in the skin layers. The model takes into account the three components of a skin specimen's BSSDF: surface reflectance, subsurface reflectance and transmittance. These components are affected by the refractive indices differences at the interfaces, tissue scattering and absorption of light by skin pigments. Due to the stochastic nature of the simulations, we use several random numbers which are uniformly distributed in the interval $[0, 1]$ and represented by $\xi_i$ for $i = 1..11$. Note that we use the subscripts $i = 1..11$ for the random numbers to disambiguate the use of one random number in one equation with another in a different equation. They are however independent random numbers and a new random number should be generated for every instance of the equation in which it is used. A flow chart is shown in Figure 4.1 to assist in visualizing the random walk process.

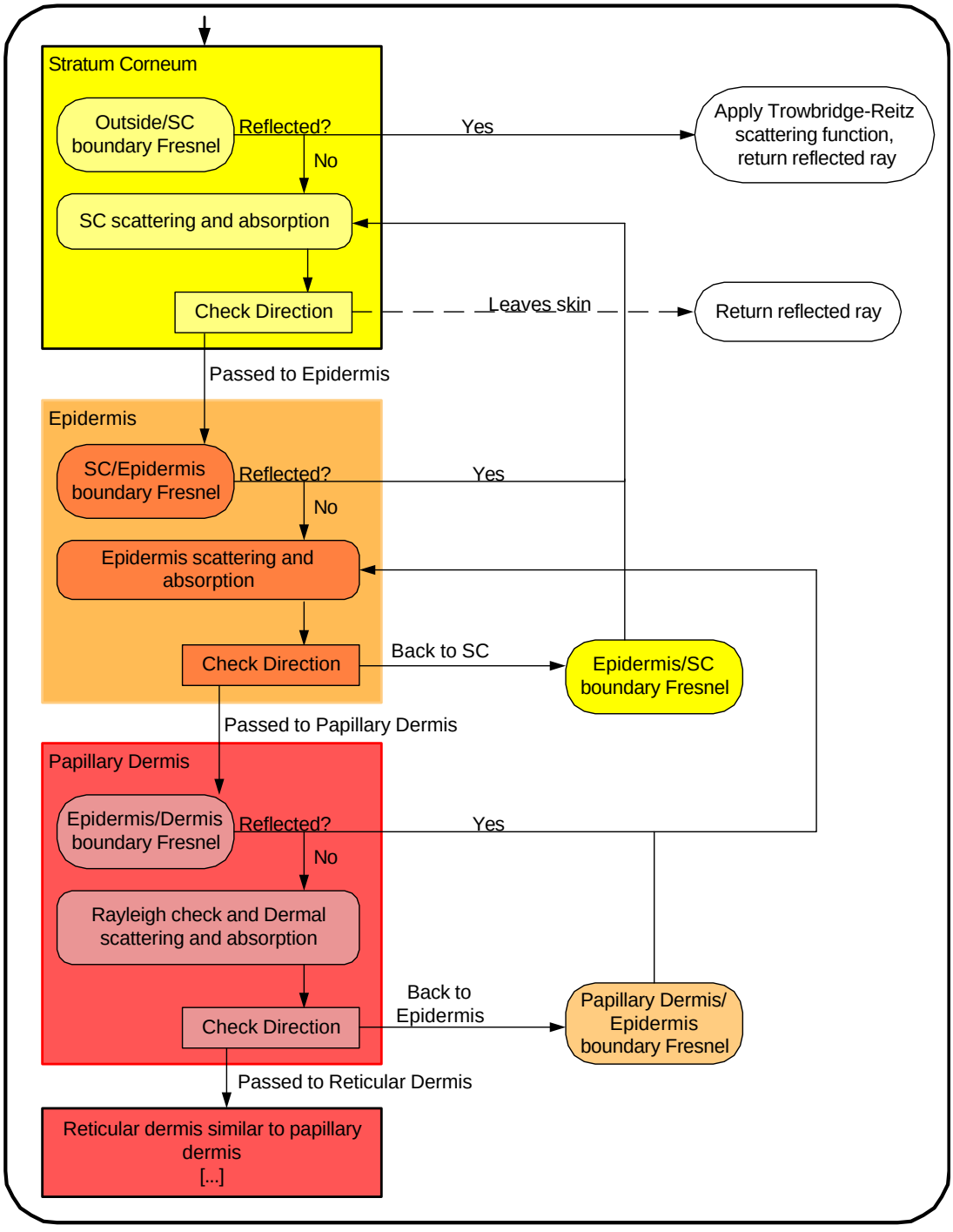


Figure 4.1: *A flow chart of the BioSpec random walk process.*

## 4.2 Input Data and Parameters

The input parameters for the BioSpec model are based on the actual biological and optical properties of human skin. Many of the parameters come directly from the biomedical literature. However, some parameters such as the concentration of hemoglobin in blood have ranges of biological plausibility. In cases such as these, we have chosen values that fit in these ranges for our evaluation. Of particular interest is our selection of values for eumelanin and phaeomelanin concentration in melanosomes. As noted by Thody *et al.*[84], phaeomelanin concentration does not have a dependency on skin type. Hence, to compute the phaeomelanin concentration, we chose a suitable average (0.15) within the ranges as given by Thody *et al.* and multiplied it by the eumelanin concentration. The eumelanin concentration was converted by selecting a value within the biologically plausible ranges as measured by Kollias and Baqer [41]. Kollias and Baqer observe in one of the 'darker' subjects, the concentration of melanin in the epidermis is 22 mg/ml (equivalent to 22 g/L). In order to derive a plausible range from this value, we can estimate a 'darkly pigmented' individual having anywhere from 18%-43% [4] of the epidermis occupied by melanosomes, giving us a biologically plausible range of 51-122 g/L as the concentration of eumelanin in melanosomes.

In addition to these parameters which are listed in Table 4.1, the BioSpec model requires the spectral molar extinction curves for the different chromophores found in human skin. The curves for oxy and deoxy hemoglobin, eumelanin, phaeomelanin, bilirubin and $\beta$-carotene were obtained from the website of the Oregon Medical Laser Center shown in Figure 2.2.

## 4.3 Reflection/Transmission at the Interfaces

The Fresnel equations [81] indicate how much light is reflected and transmitted at a plane surface as a function of the angle of incidence ($\theta_i$) and the refractive indices of the incidence and transmissive media. Hence, the computation of the Fresnel coefficients requires the refractive indices of the stratum corneum, epidermis, papillary dermis and reticular dermis, which are denoted by $\eta_s$, $\eta_e$, $\eta_p$ and $\eta_r$ respectively.

| Parameter | Symbol | Default Value | Source |
|---|---|---|---|
| Radius of Collagen fibers | $r$ | $25nm$ | [47] |
| IOR of Stratum Corneum | $\eta_s$ | 1.55 | [3] |
| IOR of Epidermis | $\eta_e$ | 1.4 | [88] |
| IOR of Papillary Dermis | $\eta_p$ | 1.36 | [37] |
| IOR of Reticular Dermis | $\eta_r$ | 1.38 | [37] |
| IOR of Collagen fibers | $\eta_f$ | 1.5 | [36] |
| Thickness of Stratum Corneum | $t_s$ | $0.001cm$ | [3] |
| Thickness of Epidermis | $t_e$ | $0.01cm$ | [3] |
| Thickness of Papillary Dermis | $t_p$ | $0.02cm$ | [3] |
| Thickness of Reticular Dermis | $t_r$ | $0.18cm$ | [3] |
| Concentration of Eumelanin in melanosomes | $c_{eu}$ | $80g/L$ | [41, 4] |
| Concentration of Phaeomelanin in melanosomes | $c_{ph}$ | $12g/L$ | [41, 84] |
| Concentration of $\beta$-carotene in SC | $c_{cs}$ | $2.1^{-4}g/L$ | [45] |
| Concentration of $\beta$-carotene in Epidermis | $c_{ce}$ | $2.1^{-4}g/L$ | [45] |
| Concentration of $\beta$-carotene in blood | $c_{cd}$ | $7.0^{-5}g/L$ | [45] |
| Concentration of hemoglobin in blood | $c_{hb}$ | $150g/L$ | [22] |
| Concentration of bilirubin in blood | $c_{bil}$ | $0.05g/L$ | [70] |
| % of Epidermis occupied by melanosomes | $\vartheta_m$ | 5.2% | [36] |
| % of Papillary Dermis composed of whole blood | $\vartheta_p$ | 1.2 % | [4] |
| % of Reticular Dermis composed of whole blood | $\vartheta_r$ | 0.91% | [4] |
| Ratio of oxy/deoxy hemoglobin | $\gamma$ | 75 % | [4] |
| Aspect ratio of folds in SC | $\sigma$ | 0.75 | [82, 83] |

Table 4.1: Input parameters of the BioSpec model and the values used in the evaluation of the model.

After computing the Fresnel coefficient ($F$) at an interface, we generate a uniform random number $\xi_1$. If $\xi_1 \leq F$, then we generate a reflected ray, otherwise we generate a refracted ray. The reflected ray is computed applying the law of reflection, and the refracted ray is computed applying Snell's law [6, 27].

## 4.4 Scattering Simulation

There are three types of scattering to consider in the BioSpec model. The first is surface reflection, which occurs when light first interacts with the surface of skin. Next, we have subsurface reflection which occurs when light continues to interact with internal skin tissues and structures. Finally, we have Rayleigh scattering which occurs when interacts with skin structures that are of approximately

the same size as the wavelength of light.

### 4.4.1 Surface Reflection

The spatial distribution of the reflected light varies according to the aspect ratio (or oblateness) of the stratum corneum folds (Section 2.2). We represent these mesostructures as ellipsoids whose aspect ratio ($\sigma \in [0,1]$) is defined as the quotient of the length of the vertical axis by the length of the horizontal axis, which are parallel and perpendicular to the specimen's normal respectively. As the folds become flatter (lower $\sigma$), the reflected light becomes less diffuse. In order to account for this effect, we perturb the reflected rays using a warping function based on a surface-structure function proposed by Trowbridge and Reitz [85], which represents rough air-material interfaces using microareas randomly curved. This surface-structure function is given by:

$$s_f = \frac{\sigma^4}{\left(\sigma^2 \cos^2 \alpha + \sin^2 \alpha\right)^2} \tag{4.1}$$

where:

$\sigma$ = oblateness of the ellipsoid representing the curved microarea,

$\alpha$ = angle between the normal of the curved microarea and the normal of the planar macrosurface.

We use this surface-structure function to compute the polar perturbation angle given by *:

$$\alpha = \arccos\left[\left(\left(\frac{\sigma^2}{\sqrt{\sigma^4 - \sigma^4\xi_2 + \xi_2}} - 1\right)\frac{1}{\sigma^2 - 1}\right)^{\frac{1}{2}}\right]. \tag{4.2}$$

The azimuthal perturbation angle is given by $\beta = 2\pi\xi_3$ since an azimuthal symmetry is assumed. BioSpec, similar to the models examined earlier, is isotropic. A more complete description of our distribution function is presented in Appendix B.

*The formula for polar perturbation that appears in the Eurographics paper describing BioSpec [42] has a typographical error, namely the position of the exponent.

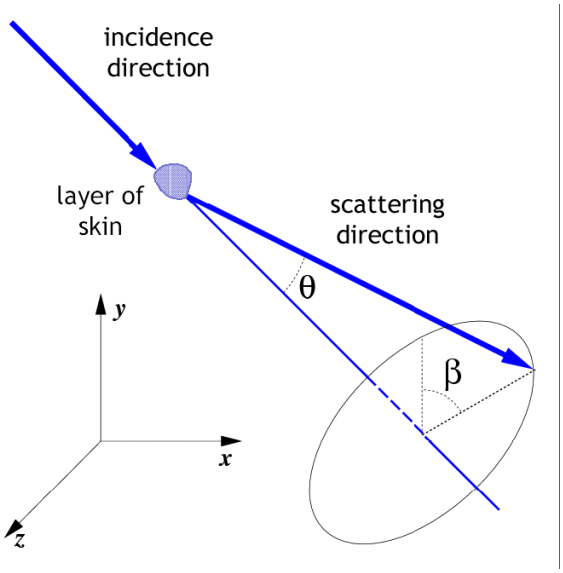


Figure 4.2: *Sketch describing the scattering angles associated with surface scattering when light interacts with a layer of skin.*

### 4.4.2 Subsurface Reflection

When a ray enters either the stratum corneum or the epidermis, it is scattered (Section 2.2). Scattering in either of these layers involves the perturbation of the incoming ray in both the polar ($\alpha_f$) and azimuthal ($\beta_f$) angles (shown in Figure 4.2). The scattering with respect to the azimuthal angle $\beta_f$ is expected to be symmetric (equal in all directions) [66], thus we use $\beta_f = 2\xi_4\pi$. The scattering direction with respect to the polar angle $\alpha_f$ is computed using a randomized table look-up algorithm. Recall that Bruns and Leun [7] have performed goniometric measurements for stratum corneum and epidermis (Section 2.2). The polar scattering angles measured at a given wavelength by Bruls and Leun [7] are stored in a table, whose access indices correspond to the measured fractions of scattered radiation. For each ray we generate a random number $\xi_5$, which we multiply by the table size. The integer part of the resulting value is used to access the corresponding polar scattering angle stored in the table. This spectral data oriented approach* provides higher accuracy results than the

*Bruls and Leun provide data for only two wavelengths. In the BioSpec model if $\lambda \leq 436nm$ we then use the 436nm scattering data, for $\lambda \geq 546nm$ we use the 546nm scattering data, and for $436nm < \lambda < 546nm$ we linearly interpolate the scattering data for 436nm and 546nm.

use of data-fitting functions [5].

It is possible for a ray to be warped such that it is reflected back to a previous layer. In this case there are few alternatives. First, we could just discard the ray, and consider it absorbed. Second, we could employ a rejection scheme to select only rays which are not reflected back to their previous layer, which avoids the inherent bias introduced in the first scheme (the bias comes from the fact that we will be substituting absorption for continued scattering which will impact the overall reflectance). Third, we could continue to follow the ray, carefully accounting for the interface change again. Though the third alternative seems the most rigorous from an optics point of view, this procedure may not be justified from a biological standpoint. Recall that scattering is occurring as a ray travels through the medium, which means that if a ray is scattered to the previous layer, it will have happened at some point through the current layer. Since the ray will have travelled some portion within the medium, we must account for the probability that it may be absorbed. This adds an order of magnitude of complexity to the random walk process which can be avoided by selecting one of the other two alternatives. According to our experiments, employing a rejection scheme to select only rays that do not get scattered to previous layers provides a higher accuracy/cost [*] ratio.

Every ray entering one of the dermal layers is initially tested for Rayleigh scattering (Section 4.4.3). The Rayleigh scattering simulation performed by the BioSpec model combines atmospheric optics [51] and skin optics [36] concepts. The Rayleigh scattering equations used by the BioSpec model is presented in the next section, with a more complete description in Appendix A.

Recall that light becomes diffuse in the dermis (Section 2.2). Hence, if the Rayleigh test fails or the ray has already been bounced off one of the dermal interfaces, then the ray is randomized around the normal direction using a warping function based on a cosine distribution [6]. [†] This warping

[*] The term 'accuracy' used here denotes the difference between the values generated by our model and the values of measured data.

[†] Although intuitively the perturbation could be performed around the direction of propagation, according to our experiments, the perturbation around the normal direction introduces less bias in the randomization, and does not require any rejection scheme for rays that may be propagated towards the upper interface. Consequently, it also provides a higher accuracy/cost ratio.

function is given in terms of the polar ($\alpha_d$) and azimuthal ($\beta_d$) perturbation angles as:

$$(\alpha_d, \beta_d) = (\arccos(\sqrt{\xi_6}), 2\pi\xi_7) \tag{4.3}$$

### 4.4.3 Rayleigh Scattering

In order to perform the Rayleigh test, we initially compute the spectral Rayleigh scattering amount (Equation 4.5), denoted by $R_{sca}(\lambda)$, which is associated with the probability that the Rayleigh scattering can occur [51]. We then generate a random number $\xi_8$. If $\xi_8 < 1 - \exp^{-R_{sca}(\lambda)}$, then the ray is scattered using polar ($\alpha_R$) and azimuthal ($\beta_R$) perturbation angles. Since the Rayleigh phase function can be assumed to be symmetric in the azimuthal direction [51], the perturbation angles are given by:

$$(\alpha_R, \beta_R) = (\psi, 2\pi\xi_{10}) \tag{4.4}$$

where the angle $\psi$ is obtained using rejection sampling in conjunction with the Rayleigh phase function [51]:

$$\begin{aligned} &do \\ &\qquad \psi = \pi\xi_9 \\ &\qquad \chi = \tfrac{3}{2}\xi_{10} \\ &while \quad (\chi > \tfrac{3}{4}(1 + \cos^2\psi)) \end{aligned}$$

According to Jacques [36], collagen fibers occupy 21% of the dermal volume, and the Rayleigh scattering in this tissue can be approximated using spheres mimicking the ultrastructure associated with the random arrays of collagen fibrils of radius $r$. This results in a fiber density given by $N = 0.21(\frac{4}{3}r^3\pi)^{-1}$, which one can use to compute the spectral Rayleigh scattering amount through the following equation:

$$R_{sca}(\lambda) = \frac{8\pi^3 \left( \left( \frac{\eta_f}{\eta_m} \right)^2 - 1 \right)^2}{3N\lambda^4} \left( \frac{t}{\cos\theta} \right) \tag{4.5}$$

where:

$\eta_f$ = index of refraction of the fibers,

$\eta_m$ = index of refraction of the dermal medium,

$t$ = thickness of the medium,

$\theta$ = angle ($< 90^\circ$) between the ray direction and the specimen's normal direction.

## 4.5 Absorption Simulation

When a ray travels in a given layer, it is first scattered as described in the previous section. The ray is then tested for absorption. If the ray is not absorbed, then it is propagated to the next layer. The absorption testing done by the BioSpec model is based on Beer's law [88]. It is performed probabilistically every time a ray starts a run in a given layer.

### 4.5.1 Free Path Length

The absorption test consists of estimating the ray free path length ($p$) through the following expression:

$$p(\lambda) = -\frac{1}{a_i(\lambda)} \ln(\xi_{11}) \cos\theta \tag{4.6}$$

where:

$a_i(\lambda)$ = total absorption coefficient of pigments of given layer $i$,

$\theta$ = angle between the ray direction and the specimen's normal direction.

If $p(\lambda)$ is greater than the thickness of the pigmented medium (both expressed in $cm$), then the ray is propagated, otherwise it is absorbed. In the BioSpec formulation the thickness of the stratum corneum, epidermis, papillary dermis and reticular dermis are denoted by $t_s$, $t_e$, $t_p$ and $t_r$ respectively.

### 4.5.2 Absorption Coefficients

The BioSpec model accounts for the presence of eumelanin, phaeomelanin, oxyhemoglobin, deoxyhemoglobin, bilirubin and $\beta$-carotene. The spectral molar extinction coefficients for these pigments, denoted $\epsilon_{eu}(\lambda)$, $\epsilon_{ph}(\lambda)$, $\epsilon_{ohb}(\lambda)$, $\epsilon_{dhb}(\lambda)$, $\epsilon_{bil}(\lambda)$ and $\epsilon_{car}(\lambda)$ respectively, are obtained from the curves shown in Figure 2.2. The total absorption coefficient for each layer is simply the sum of the absorption coefficient* for each pigment present in the layer, which is obtained by multiplying the pigment's spectral molar extinction coefficient by its estimated concentration in the layer.

It is difficult to accurately determine the baseline absorption coefficient for pigmentless skin tissues. Furthermore, due to its low magnitude [71] compared to the absorption coefficients of the skin chromophores, skin optics researchers usually assume that its effects are negligible [4]. For the sake of completeness, however, we include the baseline skin absorption coefficient ($a_{base}(\lambda)$) in the absorption equations.

The stratum corneum total absorption coefficient is given by:

$$a_1(\lambda) = a_{base}(\lambda) + a_{cs}(\lambda) \tag{4.7}$$

where:

$a_{cs}(\lambda)$ = $\beta$-carotene absorption coefficient.

The stratum corneum absorption coefficient $a_{cs}$ is given by:

$$a_{cs}(\lambda) = \frac{\epsilon_{car}(\lambda)}{537} c_{cs} \tag{4.8}$$

where:

$537$ = molecular weight of beta-carotene ($g/mole$),

$c_{cs}$ = $\beta$-carotene concentration in the stratum corneum ($\frac{g}{L}$).

*When we mention absorption coefficient in the BioSpec formulation, we are referring to the specific absorption coefficient of the pigment itself, instead of the absorption of the tissue.

The epidermis total absorption coefficient is given by:

$$a_2(\lambda) = (a_{eu}(\lambda) + a_{ph}(\lambda))\,\vartheta_m + (a_{base}(\lambda) + a_{ce}(\lambda))(1 - \vartheta_m) \tag{4.9}$$

where:

$a_{eu}(\lambda)$ = eumelanin absorption coefficient,

$a_{ph}(\lambda)$ = phaeomelanin absorption coefficient,

$a_{ce}(\lambda)$ = $\beta$-carotene absorption coefficient in the epidermis,

$\vartheta_m$ = volume fraction (%) of the epidermis occupied by melanosomes $\div 100$.

The absorption coefficient for eumelanin is given by:

$$a_{eu}(\lambda) = \epsilon_{eu}(\lambda) c_{eu} \tag{4.10}$$

where:

$c_{eu}$ = eumelanin concentration ($\frac{g}{L}$).

Similarly, the absorption coefficient for phaeomelanin ($a_{ph}(\lambda)$) is computed by multiplying its spectral molar extinction coefficient ($\epsilon_{ph}(\lambda)$) by its concentration ($c_{ph}$). Also, the absorption coefficient $a_{ce}$ is obtained by replacing $c_{cs}$ by the concentration of $\beta$-carotene ($c_{ce}$) in the epidermis in Equation 4.8.

The papillary dermis total absorption coefficient is given by:

$$a_3 = (a_{ohb}(\lambda) + a_{dhb}(\lambda) + a_{cd}(\lambda) + a_{bil}(\lambda))\,\vartheta_p + a_{base}(\lambda)(1 - \vartheta_p) \tag{4.11}$$

where:

$a_{ohb}(\lambda)$ = oxyhemoglobin absorption coefficient,

$a_{dhb}(\lambda)$ = deoxyhemoglobin absorption coefficient,

$a_{cd}(\lambda)$ = $\beta$-carotene absorption coefficient in the dermal layers,

$a_{bil}(\lambda)$ = bilirubin absorption coefficient,

$\vartheta_p$ = volume fraction (%) of the papillary dermis occupied by whole blood $\div 100$.

The absorption coefficient $a_{cd}$ is obtained by replacing $c_{cs}$ by the concentration of $\beta$-carotene in the dermal layers ($c_{cd}$) in Equation 4.8. Also, recall that the volume fractions of blood vary within the dermis tissue. Hence, to compute the reticular dermis total absorption coefficient ($a_4$), we replace $\vartheta_p$ by $\vartheta_r$ (volume fraction (%) of the reticular dermis occupied by whole blood $\div 100$) in Equation 4.11.

The absorption coefficient for oxyhemoglobin is given by:

$$a_{ohb}(\lambda) = \frac{\epsilon_{ohb}(\lambda)}{66500} c_{hb} * \gamma \tag{4.12}$$

where:

$66500$ = molecular weight of hemoglobin ($g/mole$),

$c_{hb}$ = concentration of hemoglobin in the blood ($\frac{g}{L}$),

$\gamma$ = ratio of oxyhemoglobin to the total hemoglobin concentration.

Similarly, the absorption coefficient for deoxyhemoglobin ($a_{dhb}(\lambda)$) is computed using its spectral molar extinction coefficient ($\epsilon_{dhb}(\lambda)$) and replacing $\gamma$ by $(1-\gamma)$ in Equation 4.12.

Finally, the absorption coefficient of bilirubin is given by:

$$a_{bil}(\lambda) = \frac{\epsilon_{bil}(\lambda)}{585} c_{bil} \tag{4.13}$$

where:

$585$ = molecular weight of bilirubin ($g/mole$),

$c_{bil}$ = bilirubin concentration ($\frac{g}{L}$).

# Chapter 5

# BioSpec Validation and Results

Usually models of light interaction with matter are evaluated by visually inspecting the images generated using such models. Clearly, such an evaluation may be biased by factors not directly related to the model. For example, a careful modeling of skin's geometrical details [31, 83] and an accurate post-processing tone reproduction [28, 15] may improve the realistic appearance of skin specimens. These aspects, however, are addressed in other important areas of research, and they are beyond the scope of this work.

A current trend is to perform comparisons between model readings and measured data so that the models can be used in a predictive manner [28]. We used this approach in this work, *i.e.*, the BioSpec model was tested as a separated unit of the rendering pipeline and the results were compared with actual measured data [20, 50, 96]. These comparisons were performed using a virtual spectrophotometer and a virtual goniophotometer [6], and reproducing the actual measurement conditions as faithfully as possible. The biophysical input data used in our experiments, unless otherwise stated in the text, is presented in Table 4.1. The default values were selected from the biologically plausible ranges as presented in literature. For comparisons where detailed characterization data was unavailable, we selected values within the biologically plausible range for the particular subject.

The computer generated images presented in the next section serve two purposes. First, to illustrate the applicability of the BioSpec model in the spectral simulation of medical conditions

associated with changes in the biophysical parameters. Second, to highlight an aspect for which measured data is scarce, namely the translucency of skin tissues. These images were rendered using a standard Monte Carlo path-tracing algorithm [27].

## 5.1 Results

Figure 5.1 presents comparisons of modeled reflectance curves provided by the BioSpec model with actual measured curves provided by Vrhel *et al.* [96] (available in the North Carolina State University (NCSU) spectra database) for lightly and moderately pigmented specimens. The measurements were performed considering $\theta_i = 45^\circ$ [96]. We can observe that the reflectance curves provided by the BioSpec model are qualitatively in agreement with the actual measured curves. The quantitative discrepancies may be due in part to the fact that the some parameters used in our simulations have to be estimated based on the overall description of the specimens (*e.g.*, in these experiments we set $\vartheta_m = 5.2\%$ and $\vartheta_m = 10\%$ for the lightly and moderately pigmented specimens respectively [4]. These values fall within the biologically plausible ranges for melanosome content in the epidermis for these two subjects as described by Angelopoulo [4].) Furthermore, the exact position of the absorption peaks of the pigments depends on the solvents in which they are dissolved, and one can expect small shifts when comparing to *in vivo* values [72].

The measured transmittance data for human skin available in the scientific literature, to the best of our knowledge, is limited to separated skin layers. Figure 5.2 presented comparisons between modeled and actual measured transmittance curves for the stratum corneum and epidermis tissues of two specimens, a moderately and a heavily pigmented one. The measured curves were provided by Everett *et al.* [20], and they were obtained at a normal angle of incidence ($\theta_i = 0^\circ$). Everett *et al.* [20] reported thickness values for the moderately pigmented ($t_s = 0.0017cm$ and $t_e = 0.0025cm$) and the heavily pigmented ($t_s = 0.0023cm$ and $t_e = 0.0021cm$) specimens. Based on their description of the specimens, we set $\vartheta_m = 9.5\%$ and $\vartheta_m = 38\%$ for the lightly and heavily specimens respectively. Again, we can observe a qualitative agreement between the modeled and the actual

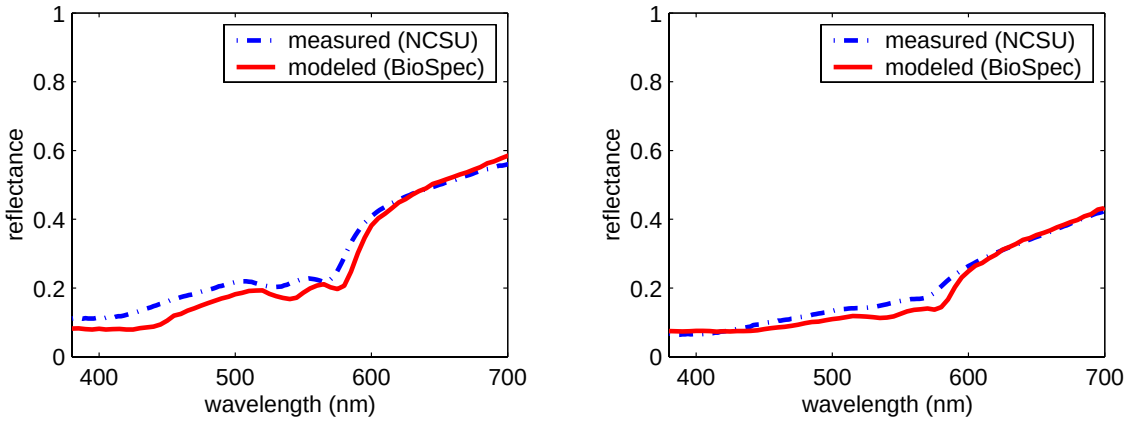


Figure 5.1: *Comparison of modeled reflectance curves provided by the BioSpec model with actual measured curves available in the NCSU spectra database by Vrhel [1994]. Left: lightly pigmented skin specimen (NCSU file 113). Right: moderately pigmented specimen (NCSU file 82).*

measured curves. The quantitative discrepancies, also related to the factors mentioned above, are noticeable but within acceptable accuracy boundaries since the measured curves have a reported tolerance of $\approx \pm 5\%$ [20].

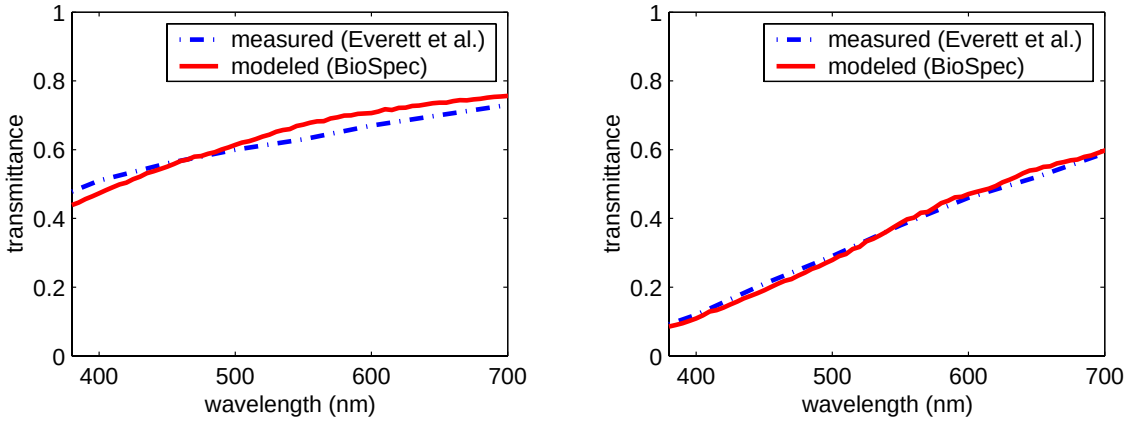


Figure 5.2: *Comparison of modeled transmittance curves (for the stratum corneum and epidermis tissues) provided by the BioSpec model with actual measured curves provided by Everett et al. [1966]. Left: moderately pigmented specimen. Right: heavily specimen.*

The overall reflectance of human skin presents interesting features. As expected, darker skin (characterized by higher volume fractions of epidermis occupied by melanosomes) reflects less light than lighter skin. However, lightly pigmented skin presents a characteristic “W” shape in

the reflectance curves between $500nm$ and $600nm$ [4]. Oxygenated hemoglobin is responsible for this feature, which can be accentuated as the proportion of oxyhemoglobin with respect to total hemoglobin increases [106]. The graphs presented in Figure 5.3 indicate that the BioSpec model can capture these optical characteristics of human skin.

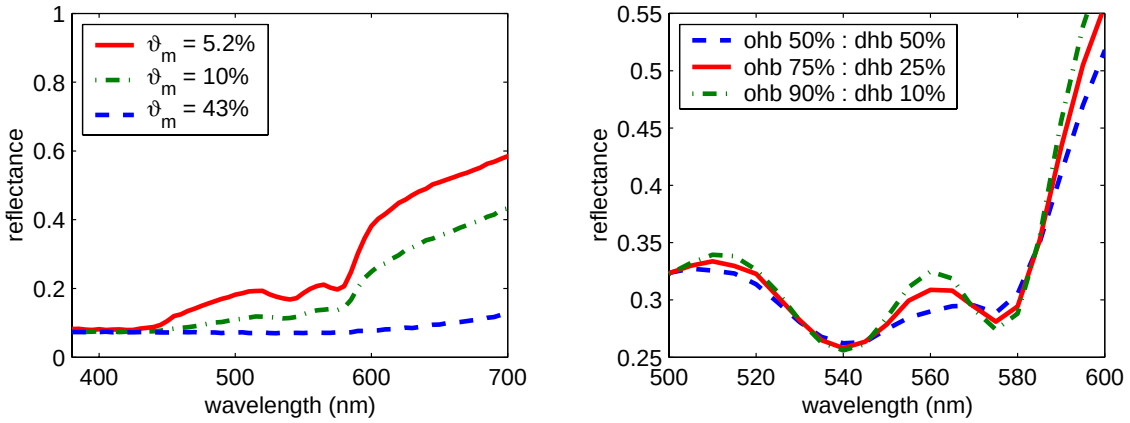


Figure 5.3: *Comparison of modeled spectral curves provided by the BioSpec model ($\theta_i = 45°$) considering the variation of biological parameters. Left: volume fractions of epidermis occupied by melanosomes ($\vartheta_m$). Right: ratio of oxygenated ($ohb$) to deoxygenated ($dhb$) hemoglobin in the dermal layers.*

Figure 5.4 shows a comparison between modeled and actual measured skin BRDFs provided by Marschner *et al.* [50]. Since the BioSpec model provides spectral readings, we needed to integrate spectral values over the visible region of the light spectrum in order to obtain data that could be compared to the data provided by Marschner *et al.* [50]. Based on the lightly pigmented specimen's description provided by Marschner *et al.* [50], we set $\vartheta_m = 2.5\%$ in these experiments. As illustrated by the measurements provided by Marschner *et al.* [50] (Figure 5.4 (left)), the BRDF of skin specimens presents an angular dependence, and it becomes more diffuse for small angles. Figure 5.4 (right) shows that the BioSpec model can represent this angular dependency, and the modeled BRDF curves generally agree with the measured BRDF curves provided by Marschner *et al.* [50]. The most noticeable quantitative discrepancies are observed for the larger angle of incidence, namely $\theta_i = 60°$. It is worth noting, however, that besides the previously mentioned factors that quantitatively affect the modeled curves, one should also consider the sources of noise in the

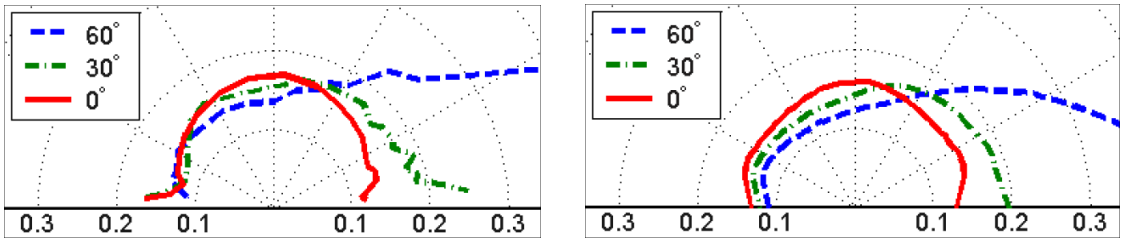


Figure 5.4: *Comparison of BRDF curves for a lightly pigmented specimen. Left: actual measured BRDF curves provided by Marschner et al. [1999]. Right: modeled BRDF curves provided by the BioSpec model.*

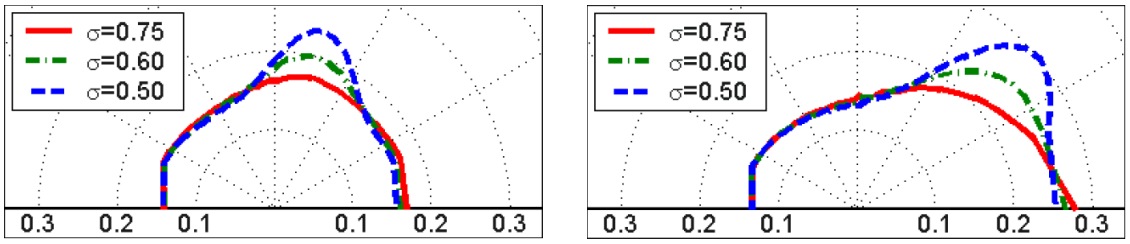


Figure 5.5: *Comparison of modeled spectral curves provided by the BioSpec model considering variations on the aspect ratio ($\sigma$) of the stratum corneum folds. Left: $\theta_i = 15°$. Right: $\theta_i = 45°$.*

measurements performed by Marschner *et al.* [50], which include deviations in the specimen's normal estimation and spatial variations in the measured BRDFs.

Skin specimens characterized by thin and numerous folds (*e.g.*, young and/or hydrated specimens) present a directional behavior stronger than specimens with wider but fewer folds (*e.g.*, old and/or dry specimens) [50, 82, 83]. The former case corresponds to folds with lower aspect ratio, while the later case corresponds to folds with a higher aspect ratio [82, 83]. Figure 5.5 presents modeled BRDF curves for two angles of incidence, namely $\theta_i = 15°$ and $\theta_i = 45°$, obtained by varying the parameter $\sigma$ associated with the folds' aspect ratio. These curves show that the BioSpec model can qualitatively simulate the variation in the scattering behavior of skin specimens associated with changes in the aspect ratio of the stratum corneum folds.

A mechanical, chemical, electrical, thermal or luminous stimulus can induce a reddening around the stimulation site on the skin. This abnormal redness of the skin, which may be also due to an inflammation [88], is caused by a dilation of the blood vessels followed by an increase in the

volume fractions of blood in the dermal layers. Figure 5.6 shows images generated to illustrate the capability of the BioSpec model of spectrally simulate this medical condition by varying, within actual biological limits, the parameters associated with the increase of the volume fractions of blood in the papillary ($\vartheta_p$) and reticular ($\vartheta_r$) dermis.

Figure 5.6: *Images generated using the BioSpec model to spectrally simulate erythema conditions. Left:* $\vartheta_p = 1.2\%$ *and* $\vartheta_r = 0.91\%$. *Center:* $\vartheta_p = 2.7\%$ *and* $\vartheta_r = 0.3\%$. *Right:* $\vartheta_p = 3.6\%$ *and* $\vartheta_r = 0.4\%$.

Jaundice, or hyperbilirubinemia [70, 71], is a medical symptom associated with the accumulation of bilirubin in the dermal tissues. It is usually caused by liver or gall bladder disorders, and it is characterized by the yellowish appearance of the skin and eyes. Figure 5.7 shows images generated to illustrate the capability of the BioSpec model of spectrally simulate this medical symptom by varying, within actual biological limits, the parameters associated with the increase of bilirubin concentration ($c_{bil}$) in the dermal layers.

The BTDF of the whole skin can be observed (*in vivo*) in body parts with a thin or absent hypodermis, such as ears, eye lids and fingers. In these areas the behavior of the transmitted light is near Lambertian, to the point where no internal structure can be noticeable [69]. Figure 5.8 presents images generated using the BioSpec model to illustrate the translucency of skin tissues as well as its variations due to different melanin pigmentation levels.

Figure 5.7: *Images generated using the BioSpec model to spectrally simulate jaundice symptoms. Left:* $c_{bil} = 0.05g/L$. *Center:* $c_{bil} = 0.5g/L$. *Right:* $c_{bil} = 3.0g/L$.

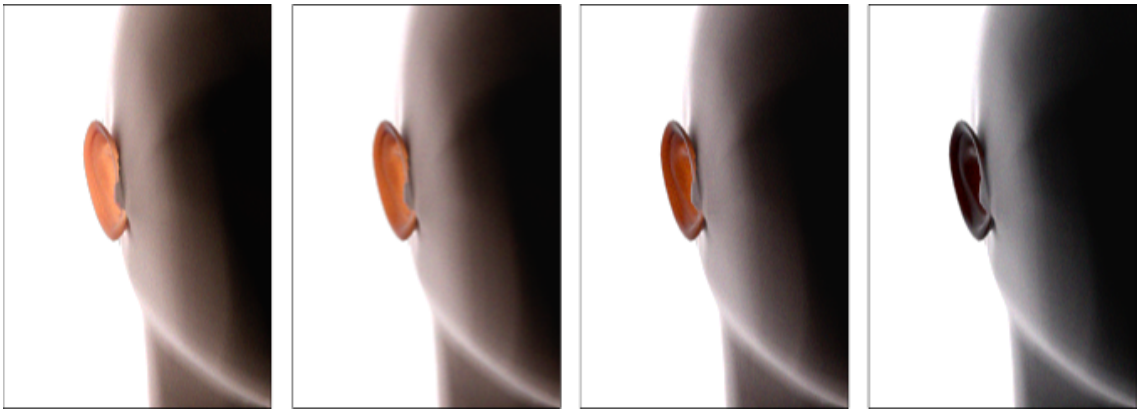

Figure 5.8: *Images generated using the BioSpec model to show variations in the translucency of skin tissues associated with different levels of melanin pigmentation. From left to right:* $\vartheta_m = 1.9\%$, $\vartheta_m = 5.2\%$ $\vartheta_m = 12\%$ *and* $\vartheta_m = 42\%$.

## 5.2 Strengths and Limitations

BioSpec, to the best of our knowledge, is the first computer graphics model capable of computing both scattering and spectral quantities for skin specimens. Its implementation based on standard Monte Carlo methods enables its straightforward integration in a variety of rendering frameworks. The algorithmic simulations performed by the model, however, are time consuming and may represent a significant bottleneck in an image synthesis pipeline. Recently, a high performance computer and cluster were efficiently combined to render animations using the BioSpec model [43]. Alterna-

tively, these simulations can be run off-line*, and the quantities computed by the model, stored and reconstructed during rendering, possibly even in real-time.

Although the simulation of surface reflection performed by the BioSpec model accounts for biological factors and employs a closer approximation to the skin mesostructures' aspect ratio than approaches based on the use of microfacets [30, 76], its generalization requires a more rigorous mathematical treatment. Similarly to previous models [30, 59, 39], shadowing and masking effects are not taking into account by the BioSpec model. Furthermore, we remark that BioSpec is a data driven model. As more data becomes available for the scattering properties of various skin layers or for the spectral properties of additional chromophores, the accuracy of the BioSpec model will increase. However, a lack of data can also result in limiting the skin conditions that can be simulated by this model.

Despite the limitations mentioned above, the scattering and spectral curves generated by the BioSpec model are in good quantitative and qualitative agreement with measured data. To date, Biospec is the only computer graphics model of light interaction with human skin to be evaluated through comparisons with spectral and scattering measured data, making it one of the few predictive models available in the computer graphics literature. Besides the experimental evaluation, rendered images were used to illustrate the applicability of the BioSpec model in the spectral simulation of medical conditions, *e.g.*, jaundice (yellowish hue) and erythema (redness), associated with changes in the biophysical parameters, and to highlight an aspect for which measured data is scarce, namely the translucency of skin tissues (Figure 5.8). The transmission of light through the whole skin can be observed in areas of the body where is the hypodermis is thin or absent. Spectrally, the light is affected by the blood present in the dermis and the melanins present in the epidermis. The distribution of this light is quite Lambertian, hence internal structure becomes indiscernible.

*Off-line refers to the precomputation of the results from the model while changing some subset of the parameters. An on-line computation using the model would mean executing the full random walk process using the complete parameter set during render time.

# Chapter 6

# Conclusions and Future Work

We presented an overview of fundamental skin optics concepts as well as a novel biophysically-based model for light interaction with human skin. It provides both spectral and scattering data for skin specimens, and it is controlled by biologically meaningful parameters. Results from the model were compared with results from actual experiments. These comparisons showed good agreement between modeled and measured data, and strengthened our confidence in the predictability of the proposed model. They also suggested that there is still room for improvement.

As future work, from a scattering point of view, we intend to investigate factors affecting the anisotropy of skin specimens, such as the presence of wrinkles. External factors, such as cosmetics, oil and sweat, may affect the skin's BRDF and light polarization. These factors will be examined in the next stage of our research as well. From a spectral point of view, we plan to extend the model's scope to the ultraviolet and infrared regions of the light spectrum and incorporate time dependent mechanisms of photon reemission. These features would allow us to use the proposed model in the visual simulation of biological processes affecting both the appearance and health of human skin such as fluorescence, tanning and the formation of melanomas.

# Bibliography


[1] ALALUF, S., HEINRICH, U., STAHL, W., TRONNIER, H., AND WISEMAN, S. Dietary carotenoids contribute to normal human skin color and uv photosensitivity. *Journal of Nutrition 132* (2002), 399–403.

[2] AMEEN, D. B., BISHOP, M. F., AND MCMULLEN, T. A lattice model for computing the transmissivity of the cornea and sclera. *Biophysical Journal 75*, 5 (November 1998), 2520–2531.

[3] ANDERSON, R., AND PARRISH, J. The optics of human skin. *Journal of Investigative Dermatology 77*, 1 (1981), 13–19.

[4] ANGELOPOULOU, E. Understanding the color of human skin. In *Human Vision and Electronic Imaging VI* (2001), SPIE, vol. 4299, pp. 243–251.

[5] BARANOSKI, G., KRISHNASWAMY, A., AND KIMMEL, B. Revisiting the foundations of subsurface scattering. Tech. Rep. CS-2003-45, School of Computer Science, University of Waterloo, December 2003.

[6] BARANOSKI, G., AND ROKNE, J. An algorithmic reflectance and transmittance model for plant tissue. *Computer Graphics Forum (EUROGRAPHICS Proceedings) 16*, 3 (September 1997), 141–150.

[7] BRULS, W., AND VAN DER LEUN, J. Forward scattering properties of human epidermal layers. *Photochem. Photobiol. 40* (1984), 231–242.

[8] BURDEN, R., AND FAIRES, J. *Numerical Analysis*, fifth ed. PWS-KENT Publishing Company, Boston, 1993.

[9] CHANDRASEKHAR, S. *Radiative Transfer*. Dover Publications Inc., New York, 1960.

[10] CHEDEKEL, M. Photophysics and photochemistry of melanin. In *Melanin: Its Role in Human Photoprotection* (Overland Park, Kansas, USA, 1995), M. C. L. Zeise and T. Fitzpatrick, Eds., Valdenmar Publishing Company, pp. 11–22. 2223b.

[11] CHEONG, W., PRAHL, S., AND WELCH, A. A review of the optical properties of biological tissues. *IEEE Journal of Quantum Electronics 26*, 12 (December 1990), 2166–2185.

[12] CHURMAKOV, D., MEGLINSKY, I., PILETSKY, S., AND GREENHALGH, D. Analysis of skin tissues spatial fluorescence distribution by the Monte Carlo simulation. *Journal of Physics D: Applied Physics 36* (July 2003), 1722–1728.

[13] COTTON, S. A noninvasive skin imaging system. Tech. Rep. CSR-97-03, School of Computer Science, The University of Birmingham, 1997.

[14] COTTON, S., AND CLARIDGE, E. Developing a predictive model of skin colouring. In *SPIE Vol. 2708, Medical Imaging 1996* (1996), pp. 814–825.

[15] DEVLIN, K., CHALMERS, A., WILKIE, A., AND PURGATHOFER, W. Tone reproduction and physically based spectral rendering. In *Eurographics - State of the Art Reports* (2002), pp. 101–123.

[16] DIFFEY, B. A mathematical model for ultraviolet optics in skin. *Physics in Medicine and Biology 28*, 6 (1983), 647–657.

[17] DOI, M., AND TOMINAGA, S. Spectral estimation of human skin color using the Kubelka-Munk theory. In *SPIE/IS&T Electronic Imaging* (2003), SPIE, vol. 5008, pp. 221–228.

[18] DOORNBOS, R., LANG, R., AALDERS, M., CROSS, F., AND STERENBORG, H. The determination of in vivo human tissue optical properties and absolute chromophore concentrations

using spatially resolved steady-state diffuse reflectance spectroscopy. *Physics in Medicine and Biology 44* (1999), 967–981.

[19] EASON, G., VEITCH, A., NISBET, R., AND TURNBULL, F. The theory of backscattering of light by blood. *Journal of Physics 11* (1978), 1463–1479.

[20] EVERETT, M., YEARGERS, E., SAYRE, R., AND OLSEN, R. Penetration of epidermis by ultraviolet rays. *Photochemistry and Photobiology 5* (1966), 533–542.

[21] FARELL, T., PATTERSON, M., AND WILSON, B. A diffusion theory model of spatially resolved, steady-state diffuse reflectance for the noninvasive determination of tissue optical properties in vivo. *Medical Physics 19* (1992), 879–888.

[22] FLEWELLING, R. Noninvasive optical monitoring. In *The Biomedical Engineering Handbook* (Boca Raton, FL, USA, 1981), J. Bronzino, Ed., IEEE Press, pp. 1–11. Section 86.

[23] FLOCK, S. T., PATTERSON, M. S., WILSON, B. C., AND WYMAN, D. R. Monte Carlo modeling of light propagation in highly scattering tissues - I: Model predictions and comparison with diffusion theory. *IEEE Transactions on Biomedical Engineering 36*, 12 (December 1989), 1162–1168.

[24] FOURTY, T., BARET, F., JACQUEMOUD, S., SCHMUCK, G., AND VERDEBOUT, J. Leaf optical properties with explicit description of its biochemical composition: Direct and inverse problems. *Remote Sensing of Environment 56* (1996), 104–117.

[25] FRETTERED, R. J., AND LONGINI, R. L. Diffusion dipole source. *Journal of the Optical Society of America 63*, 3 (1973), 336–337.

[26] FURUTSO, K. Diffusion equation derived from space-time transport equation. *Journal of the Optical Society of America 70* (1980), 360.

[27] GLASSNER, A. *Principles of Digital Image Synthesis.* Morgan Kaufmann Publishers, Inc, San Francisco, 1995.

[28] GREENBERG, D., ARVO, J., LAFORTUNE, E., TORRANCE, K., FERWERDA, J., WALTER, B., TRUMBORE, B., SHIRLEY, P., PATTANAIK, S., AND FOO, S. A framework for realistic image synthesis. In *SIGGRAPH, Annual Conference Series* (1997), pp. 477–494.

[29] HAEGHEN, Y. V., NAEYAERT, J., LEMAHIEU, I., AND PHILIPS, W. An imaging system with calibrated color image acquisition for use in dermatology. *IEEE Transactions on Medical Imaging 19*, 7 (July 2003), 722–730.

[30] HANRAHAN, P., AND KRUEGER, W. Reflection from layered surfaces due to subsurface scattering. In *SIGGRAPH, Annual Conference Series* (August 1993), pp. 165–174.

[31] HARO, A., GUENTER, B., AND ESSA, I. Real-time, photo-realistic, physically based rendering of fine scale human skin structure. In *Rendering Techniques'2001 (Proceedings of the 12th Eurographics Rendering Workshop)* (London, June 2001), P. M. Hanrahan and W. Purgathofer, Eds., Springer-Verlag, pp. 53–62.

[32] HIRKO, R. J., FRETTERD, R. J., AND LONGINI, R. L. Application of the diffusion dipole to modelling the optical characteristics of blood. *Medical and Biological Engineering 13*, 2 (1975), 192–195.

[33] HUNTER, R., AND HAROLD, R. *The Measurement of Appearance*, second ed. John Wiley & Sons, New York, 1987.

[34] ISHIMARU, A. *Wave Propagation and Scattering in Random Media*, vol. 1. IEEE Press, New York, 1978.

[35] ISHIMARU, A. *Wave Propagation and Scattering in Random Media*, vol. 2. IEEE Press, New York, 1978.

[36] JACQUES, S. Origins of tissue optical properties in the uva visible and nir regions. *OSA TOPS on Advances in Optical Imaging and Photon Migration 2* (1996), 364–369.

[37] JACQUES, S., ALTER, C., AND PRAHL, S. Angular dependence of HeNe laser light scattering by human dermis. *Lasers in Life Sciences 1*, 4 (1987), 309–333.

[38] JENSEN, H., AND BUHLER, J. A rapid hierarchical rendering technique for translucent materials. In *SIGGRAPH, Annual Conference Series* (July 2002), pp. 576–581.

[39] JENSEN, H., MARSCHNER, S., LEVOY, M., AND HANRAHAN, P. A practical model for subsurface light transport. In *SIGGRAPH, Annual Conference Series* (August 2001), pp. 511–518.

[40] JIN, Z., AND STAMMES, K. Radiative transfer in nonuniformly refracting layered media: atmosphere-ocean system. *Applied Optics 33*, 3 (January 1994), 431–442.

[41] KOLLIAS, N., AND BAQER, A. On the assesssment of melanin in human skin in vivo. *Photochemistry and Photobiology 43*, 1 (1986), 49–54.

[42] KRISHNASWAMY, A., AND BARANOSKI, G. A biophysically-based spectral model of light interaction with human skin. *Computer Graphics Forum (EUROGRAPHICS Proceedings) 23*, 4 (2004), 331–340.

[43] KRISHNASWAMY, A., AND BARANOSKI, G. Combining a shared-memory high performance computer and a heterogeneous cluster for the simulation of light interaction with human skin. *Proceedings of the 16th Symposium on Computer Architecture and High Performance Computing* (2004), 166–171. Foz do Iguau, Parana, Brazil.

[44] KUBELKA, P., AND MUNK, F. Ein beitrag zur optik der farbanstriche. *Zurich Tech. Physik 12* (1931), 543.

[45] LEE, R., MATHEWS-ROTH, M., PATHAK, M., AND PARRISH, J. The detection of carotenoid pigments in human skin. *Journal of Investigative Dermatology 64* (1975), 175–177.

[46] LENOBLE, J. *Atmospheric Radiative Transfer*. A. Deepak Publishing, Hampton, Virginia, USA, 1993.

[47] LI, S. Biologic biomaterials: Tissue-derived biomaterials (collagen). In *Biomaterials Principles and Applications* (Boca Raton, USA, 2003), J. Park and J. Bronzano, Eds., CRC Press, pp. 117–139.

[48] LIOU, K.-N. *Introduction to Atmospheric Radiation (2nd. Edition)*. Elsevier Science, San Diego, 2002.

[49] MARSCHNER, S., JENSEN, H., CAMMARANO, M., WORLEY, S., AND HANRAHAN, P. Light scattering from human hair fibers. *ACM Transactions on Graphics 22*, 3 (2003), 780–791.

[50] MARSCHNER, S., WESTIN, S. H., LAFORTUNE, E., TORRANCE, K., AND GREENBERG, D. Image-based brdf measurement including human skin. In *Rendering Techniques'1999 (Proceedings of the 10th Eurographics Rendering Workshop)* (Granada, June 1999), D. Lischinski and G. W. Larson, Eds., Springer-Verlag, pp. 119–130.

[51] MCCARTNEY, E. *Optics of the Atmosphere: Scattering by Molecules and Particles*. John Wiley & Sons Inc., 1976.

[52] MEGLINSKY, I., AND MATCHER, S. Modelling the sampling volume for skin blood oxygenation. *Medical & Biological Engineering & Computing 39* (2001), 44–49.

[53] MEGLINSKY, I., AND MATCHER, S. Computer simulation of the skin reflectance spectra. *Computer Methods and Programs in Biomedicine 70* (2003), 179–186.

[54] METROPOLIS, N., AND ULAM, S. The Monte Carlo method. *Journal of the American Statistical Association 44*, 247 (September 1949), 335–341.

[55] MONCRIEFF, M., COTTON, S., HALL, P., SCHIFFNER, R., LEPSKI, U., AND CLARIDGE, E. Siascopy assists in the diagnosis of melanoma by utilising computer vision techniquesto

visualise internal structures of the skin. *Medical Image Understanding and Analysis* (2001), 53–56.

[56] MOURANT, J., FREYER, J., HIELSCHER, A., EICK, A., SHEN, D., AND JOHNSON, T. Mechanisms of light scattering from biological cells relevant to noninvasive optical-tissue diagnostics. *Applied Optics 37*, 16 (June 1998), 3586–3593.

[57] NAKAI, H., MANABE, Y., AND INOKUCHI, S. Simulation analysis of spectral distributions of human skin. In *14th International Conference on Pattern Recognition* (1998), pp. 1065–1067.

[58] NAKAO, D., TSUMURA, N., AND MIYAKE, Y. Real-time multi-spectral image processing for mapping pigmentation in human skin. *Medical Imaging Technology 20*, 2 (2002), 123–133.

[59] NG, C., AND LI, L. A multi-layered reflection model of natural human skin. In *Computer Graphics International 2001* (Hong Kong, July 2001), pp. 249–256.

[60] NICODEMUS, F., RICHMOND, J., HSIA, J., GINSBERG, I., AND LIMPERIS, T. Geometrical considerations and nomenclature for reflectance. In *Physics-Based Vision Principles and Practice: Radiometry* (Boston, 1992), L. Wolff, S. Shafer, and G. Healey, Eds., Jones and Bartlett Publishers, pp. 94–145.

[61] NISCHIK, M., AND FORSTER, C. Analysis of skin erythema using true-color images. *IEEE Transactions on Medical Imaging 16*, 6 (December 1997), 711–716.

[62] NISHITA, T., SIRAI, T., TADAMURA, K., AND NAKAMAE, E. Display of the earth taking into account atmospheric scattering. *SIGGRAPH, Annual Conference Series* (1993).

[63] PARSAD, D., WAKAMATSU, K., KANWAR, A., KUMAR, B., AND ITO, S. Eumelanin and phaeomelanin contents of depigmented and repigmented skin in vitiligo patients. *British Journal of Dermatology 149* (2003), 624–626.

[64] PENNDORF, R. Tables of the Refractive Index for standard Air and the Rayleigh Scattering Coefficient for the Spectral Region between 0.2 and 20.0 mgr and Their Application to Atmospheric Optics. *Journal of the Optical Society of America (1917-1983) 47* (Feb. 1957), 176–+.

[65] PRAHL, S. *Light Transport in Tissue*. PhD thesis, The University of Texas at Austin, TX, USA, December 1988.

[66] PRAHL, S., KEIJZER, M., JACQUES, S., AND WELCH, A. A Monte Carlo model of light propagation in tissue. *SPIE Institute Series IS 5* (1989), 102–111.

[67] PRAHL, S., VAN GEMERT, M., AND WELCH, A. Determining the optical properties of turbid media using the adding-doubling method. *Applied Optics 32*, 4 (1993), 559–568.

[68] PURGATHOFER, W. Open issues in photo-realistic rendering. In *Computer Graphics Forum (EUROGRAPHICS Proceedings)* (2003), p. xix. Invited talk.

[69] RODRIGUEZ, J., YAROSLAVSKY, I., YAROSLAVSKY, A., BATTARBEE, H., AND TUCHIN, V. Time-resolved imaging in diffusive media. In *Handbook of Optical Biomedical Diagnostics* (Bellingham, WA, USA, 2002), V. Tuchin, Ed., SPIE Press, pp. 357–404.

[70] ROLINSKY, B., KÜSTER, H., UGELE, B., GRUBER, R., AND HORN, K. Total bilirubin measurement by photometry on a blood gas analyser: potential for use in neonatal testing at point of care. *Clinical Chemistry 47*, 10 (2001), 1845–1847.

[71] SAIDI, I. *Transcutaneous optical measurement of hyperbilirubinemia in neonates*. PhD thesis, Rice University, Houston, Texas, USA, 1994.

[72] SALISBURY, F., AND ROSS, C. *Plant Physiology*, third ed. Wadsworth Publishing Company, Belmont, California, 1985.

[73] SARDAR, D., AND LEVY, L. Optical properties of whole blood. *Lasers in Medical Science 13* (1998), 106–111.

[74] SHIMADA, M., YAMADA, Y., ITOH, M., AND YATAGAI, T. Melanin and blood concentration in human skin studied by multiple regression analysis: assessment by Monte Carlo simulation. *Physics in Medicine and Biology 46* (2001), 2397–2406.

[75] SIMPSON, C., KOHL, M., ESSENPREIS, M., AND COPE, M. Near infrared optical properties of ex-vivo human skin and subcutaneous tissues measured using the Monte Carlo inversion technique. *Physics in Medicine and Biology 43* (1998), 2465–2478.

[76] STAM, J. An illumination model for a skin layer bounded by rough surfaces. In *Rendering Techniques'2001 (Proceedings of the 12th Eurographics Rendering Workshop)* (London, June 2001), P. M. Hanrahan and W. Purgathofer, Eds., Springer-Verlag, pp. 39–52.

[77] STAMNES, K., AND CONKLIN, P. A new multi-layer discrete ordinate approach to radiative transfer in vertically inhomogeneous atmospheres. *Journal of Quantum Spectroscopy and Radiative Transfer 31*, 3 (1984), 273–282.

[78] STEINKE, J., AND SHEPHERD, A. Diffusion model of the optical absorbance of whole blood. *Journal of the Optical Society of America 5*, 6 (1988), 813–822.

[79] STRUTT, J. On the scattering of light by small particles. *Philosophical Magazine 41*, 275 (June 1871), 447–454.

[80] STRUTT, J. On the transmission of light through an atmosphere containing many small particles in suspension, and on the origin of the blue of the sky. *Philosophical Magazine 47* (1899), 375–384.

[81] SU, Y., WANG, W., XU, K., AND JIANG, C. The optical properties of skin. In *Optics in Health Care and Biomedical Optics: Diagnostics and Treatment* (2002), SPIE, vol. 4916, pp. 299–304.

[82] TALREJA, P., KASTING, G., KLEENE, N., PICKENS, W., AND WANG, T. Visualization of the lipid barrier and measurement of lipid pathlength in human stratum corneum. *AAPS PharmSCi 3*, 2 (2001), 1–9.

[83] THALMANN, N., KALRA, P., LÉVÊQUE, J., BAZIN, R., BATISSE, D., AND QUERLEUX, B. A computational skin model: fold and wrinkle formation. *IEEE Transactions on Information Technology in Biomedicine 6*, 4 (2002), 317–323.

[84] THODY, A., HIGGINS, E., WAKAMATSU, K., ITO, S., BURCHILL, S., AND MARKS, J. Pheomelanin as well as eumelanin is present in human dermis. *Journal of Investigative Dermatology 97* (1991), 340–344.

[85] TROWBRIDGE, T., AND REITZ, K. Average irregularity representation of a rough surface for ray reflection. *Journal of the Optical Society of America 65*, 5 (May 1975), 531–536.

[86] TSUMURA, N., KAWABUCHI, M., HANEISHI, H., AND MIYABE, Y. Mapping pigmentation in human skin by multi- visible-spectral imaging by inverse optical scattering technique. In *IS&T/SID Eighth Color Imaging Conference* (2000), pp. 81–84.

[87] TSUMURA, N., OJIMA, N., SATO, K., SHIRAISHI, M., SHIMIZU, H., NABESHIMA, H., AKAZAKI, S., HORI, K., AND MIYAKE, Y. Image-based skin color and texture analysis/synthesis by extracting hemoglobin and melanin information in the skin. In *SIGGRAPH, Annual Conference Series* (2003).

[88] TUCHIN, V. *Tissue Optics Light Scattering Methods and Instruments for Medical Diagnosis*. The International Society for Optical Engineering, Bellingham, WA, USA, 2000.

[89] TUCHIN, V., UTZ, S., AND YAROSLAVSKY, I. Tissue optics, light distribution, and spectroscopy. *Optical Engineering 33* (1994), 3178–3188.

[90] VAN DE HULST, H. *Multiple Light Scattering: Tables, Formulas, and Applications*, vol. 1. Academic Press, New York, 1980.

[91] VAN DE HULST, H. *Multiple Light Scattering: Tables, Formulas, and Applications*, vol. 2. Academic Press, New York, 1980.

[92] VAN DE HULST, H. *Light Scattering by Small Particles*, 2nd ed. Dover Publications Inc., New York, 1981.

[93] VAN GEMERT, M., JACQUES, S., STERENBORG, H., AND STAR, W. Skin optics. *IEEE Transactions on Biomedical Engineering 36*, 12 (1989), 1146–1154.

[94] VAN GEMERT, M., AND STAR, W. Relations between the Kubelka-Munk and the transport equation models for anisotropic scattering. *Laser in the Life Sciences 1*, 4 (1987), 287–298.

[95] VAN GEMERT, M., WELCH, A., AND STAR, W. Tissue optics for a slab geometry in diffusion approximation. *Laser in the Life Sciences 2* (1987), 295–302.

[96] VRHEL, M., GERSHON, R., AND IWAN, L. Measurement and analysis of object reflectance spectra. *Color Research and Application 19*, 1 (1994), 4–9.

[97] WAN, S., ANDERSON, R., AND PARRISH, J. Analytical modeling for the optical properties of the skin with in vitro and in vivo appplications. *Photochemistry and Photobiology 34* (1981), 493–499.

[98] WANG, L., AND JACQUES, S. Hybrid method of Monte Carlo simulation and diffusion theory for light reflectance by turbid media. *Optical Society of America 10*, 8 (1995), 1746–1752.

[99] WANG, L., JACQUES, S., AND ZHENG, L. MCML – Monte Carlo modelling of light transport in multi-layered tissues. *Computer methods and programs in biomedicine* (1995).

[100] WILSON, B., AND ADAM, G. A Monte Carlo model for the absorption and flux distributions of light in tissue. *Medical Physics 10* (1983), 824–830.

[101] YAROSLAVSKY, A., PRIEZZHEV, A., RODRIGUEZ, J., YAROSLAVSKY, I., AND BATTARBEE, H. Optics of blood. In *Handbook of Optical Biomedical Diagnostics* (Bellingham, WA, USA, 2002), V. Tuchin, Ed., SPIE Press, pp. 169–216.

[102] YAROSLAVSKY, A., UTZ, S., TATARINTSEV, S., AND TUCHIN, V. Angular scattering properties of human epidermal layers. In *Human Vision and Electronic Imaging VI* (1994), SPIE, vol. 2100, pp. 38–41.

[103] YOON, G. *Absorption and Scattering of Laser Light in Biological Media - Mathematical Modeling and Methods for Determining Optical Properties*. PhD thesis, University of Texas at Austin, USA, 1988.

[104] YOON, G., PRAHL, S., AND WELCH, A. Accuracies of the diffusion approximation and its similarity relations for laser irradiated biological media. *Applied Optics 28*, 12 (1989), 2250–2255.

[105] YOON, G., WELCH, A., MOTAMEDI, M., AND VAN GEMERT, M. Development and application of three-dimensional light distribution model for laser irradiated tissue. *IEEE Journal of Quantum Electronics QE-23* (1987), 1721–1733.

[106] ZONIOS, G., BYKOWSKY, J., AND KOLLIAS, N. Skin melanin, hemoglobin, and light scattering properties can be quantitatively assessed in vivo using diffuse reflectance spectroscopy. *Journal of Investigative Dermatology 117*, 6 (2001), 1452–1457.

# Index

# Appendix A

# Rayleigh Scattering

In this appendix, we present a description of the Rayleigh scattering equations used in the BioSpec model. This description should highlight the steps taken to go from the basics of Rayleigh scattering theory to Equation 4.5. We begin by presenting equations for single scattering. We then discuss the Rayleigh phase function and scattered intensity. We finally present equations for computing volume Rayleigh scattering.

## A.1 Single Scattering

The fundamentals of light scattering begins by examining the event of light scattering with a single particle*. One of the fundamental assumptions that should be made in order to consider single scattering is independence [92]. This means that the particles in a medium are far enough apart that the interaction of light with one particle is not affected by another nearby particle.

The combination of the scattering and absorption cross sections gives the attenuation cross section represented by:

*The particle we are referring to is a small particle with finite mass such as a molecule, but not a light particle (photon).

$$R_{att}(\lambda) = R_{abs}(\lambda) + R_{sca}(\lambda) \tag{A.1}$$

where:

$R_{att}$ = attenuation cross section,

$R_{abs}$ = absorption cross section,

$R_{sca}$ = scattering cross section.

The general Rayleigh scattering cross section is given by:

$$R_{sca}(\lambda) = \frac{8}{3}\pi k^4 \left|\alpha^2\right| \tag{A.2}$$

where:

$R_{sca}$ = scattering cross section,

$k$ = wave number (propagation constant in vacuum) $k = \frac{2\pi}{\lambda}$,

$\alpha$ = polarizability.

Note that Equation A.2 makes no assumptions about the shape of the particles (represented in the $\alpha$ (polarizability) term).

The absorption cross section for general Rayleigh scattering is given by:

$$R_{abs}(\lambda) = 4\pi k \varrho(i\alpha) \tag{A.3}$$

where:

$\varrho(i\alpha)$ = complex portion of index of refraction of particle describing permeability.

Again, note that Equation A.3 makes no assumption about the shape of the particles either.

The polarizability mentioned in Equation A.2 refers to particle polarizability which is affected by the shape and orientation of the particle, and it should not be confused with the polarization of the wave. It is worth noting that the Rayleigh scattering cross section is only valid for particles with relatively small radius ($r < 0.05\lambda$, where $r$ is the radius of the particle and $lambda$ is the

wavelength of light) [34, 35].

Lord Rayleigh (J.W. Strutt, third Baron of Rayleigh) originally proposed his equations considering dielectric particles [79, 80] which exhibit both scattering and absorption. However, models in atmospheric optics omit the absorption cross section due to its negligible impact and its complexity [46, 51, 62]. We also choose to omit the absorption cross section with collagen fibers, since the absorption due to collagen fibers is negligible [2].

## A.2 Phase Function

The phase function mathematically approximates the deflection trajectories of rays when they interact with a particle [92, 90, 91]. A phase function is a probability density function that, when given the relative outgoing angle of a deflected particle, describes the probability of the particle being deflected in that direction. As with any probability density function, the phase function, in order to be energy conserving, must be normalized to unity and satisfy the following equation:

$$\int_{\Omega} \frac{1}{4\pi} p(\cos\theta) d\Omega = 1 \tag{A.4}$$

where:

$p(\cos\theta)$ = probability of light being scattered in the direction given by the outgoing angle $\theta$.

The Rayleigh phase function for unpolarized light is given by [9]:

$$p(\cos\theta) = \frac{3}{4}\left(1 + \cos^2(\theta)\right) \tag{A.5}$$

## A.3 Scattered Intensity

The intensity of the light scattered in one direction due to Rayleigh scattering is shown in the following equation [92]:

$$I = I_o \frac{\left(1 + cos^2\Theta\right) k^4 \left|\alpha^2\right|}{2d^2} \tag{A.6}$$

where:

$I$ = intensity of scattered light,

$I_o$ = intensity of incident light,

$\Theta$ = scattering angle,

$d$ = distance to the center of the particle.

For particles that are spherical, we can describe the isotropic polarizability ($\alpha$) as [92]:

$$\alpha = \frac{m^2 - 1}{m^2 + 2} r^3 \tag{A.7}$$

where:

$m$ = complex refractive index of the particle (=$\infty$ for totally reflecting spheres),

$r$ = radius of the particle.

By substituting $\frac{2\pi}{\lambda}$ for $k$ and Equation A.7 into Equation A.6, we get the following equation describing the Rayleigh scattering function for spherical particles and incident unpolarized light:

$$I = I_o \frac{8\pi^4 (1 + \cos^2\Theta)}{r^2 \lambda^4} \left| \left( \frac{m^2 - 1}{m^2 + 2} a^3 \right)^2 \right| \tag{A.8}$$

We can see that this intensity has the characteristic $\lambda^4$ dependency. This representation of scattered intensity is useful when trying to evaluate the amount of the incident light that is scattered in a particular direction. Due to the algorithmic nature of the BioSpec model, this expression is not needed in its implementation.

## A.4 Volume Scattering

The single scattering event describes the process of scattering when light interacts with a single particle. In the case of a medium such as collagen, the small size of the particles makes the sim-

ulation of the interaction of light with every particle in the medium impractical. In order to make the problem more tractable, some simplifications and assumptions are essential so that the entire volume containing the particles can be considered.

If we assume that the individual particles within a volume are far enough away from each other so that scattering due to one particle does not affect the scattering due to another, and that the distribution of these particles is random and homogeneous within the volume, then the effects of single particle scattering can be aggregated over the volume [34, 35]. One way of performing this aggregation is to compute the attenuation ratio per unit length and apply Bouger's law. Given this attenuation ratio and the amount travelled in the medium, one can compute the scattering probability of a given ray. However, in order to compute the attenuation ratio, one must know the amount of particles within the volume. This technique, called optical path, or optical depth, has been applied in several atmospheric scattering models [46], and it has been adapted for collagen fibers [36].

Researchers in atmospheric optics assume that the molecules are opaque. One can apply the same assumption for collagen fibers. By using the same formulation used in atmospheric optics to derive the scattering coefficient for a volume of air [46], one can obtain the scattering coefficient for a volume of collagen fibers. In other words, if we take Equation A.2 and substitute $\frac{2\pi}{\lambda}$ for $k$, and if we also assume the effects of scattering aggregate (or accumulate)* over all the particles in a volume, we get:

*We can assume that effect of scattering accumulates over a volume of particles, since independence guarantees that an interaction with one particle does not interfere with interaction with another particle.

$$R_{sca}(\lambda) = \frac{128\pi^5}{3\lambda^4 N} |\alpha|^2 \tag{A.9}$$

where:

$N$ = number of particles in the volume (because of aggregate effect).

Now, we can apply the Lorentz-Lorenz formula [92] to derive a value of $\alpha$ for isotropic spheres whose mutual distances are small compared to $\lambda$. The Lorentz-Lorenz formula is given by:

$$\alpha = \frac{3}{4\pi N} \frac{m^2 - 1}{m^2 + 2} \tag{A.10}$$

where:

$N$ = number of molecules per unit volume.

However, the complex portion of the index of refraction still poses a problem. In atmospheric radiative transfer the polarizability can be approximated by [48]:

$$\alpha = \frac{1}{4\pi N}(\eta^2 - 1) \tag{A.11}$$

where:

$\eta$ = real refractive index of the particle.

By using the approximated polarizability factor, the scattering (and thus attenuation) cross section becomes:

$$R_{sca}(\lambda) = \frac{8\pi^3 N \left(\eta^2 - 1\right)^2}{3\lambda^4 N^2} f(\delta) \tag{A.12}$$

where:

$f(\delta)$ = anisotropy factor function.

It is worth noting that one still needs to account for the varying index of refraction within the volume. For this purpose, the anisotropy factor function is introduced in atmospheric optics:

$$f(\delta) = \frac{(6 + 3\delta)}{(6 - 7\delta)} \tag{A.13}$$

where:

$\delta$ = anisotropic factor of 0.035 to account for varying index of refraction [64].

However, we have no evidence to suggest that this anisotropic factor is necessary or relevant for collagen fibres. Hence, for the sake of simplicity, it is not used in our formulation, which results in:

$$R_{sca}(\lambda) = \frac{8\pi^3 N(\eta^2 - 1)^2}{3\lambda^4 N^2} \tag{A.14}$$

Using this cross section, we can determine the total scattering coefficient by a unit volume of collagen fibers. Researchers in atmospheric optics assume the index of refraction of the medium is that of a vacuum, which is why in Equation A.14 the real index of refraction is presented by $\eta$ alone (expanded, it would be $\frac{\eta}{1.0}$, where 1.0 is the index of refraction of vacuum). In the dermis, however, the collagen fibers are suspended in a medium with its own index of refraction. Therefore, we must represent the index of refraction of this medium. In addition, note that the $N$ term in the numerator can be cancelled. Performing these two operations we get:

$$R_{sca}(\lambda) = \frac{8\pi^3 (\left(\frac{\eta_f}{\eta_m}\right)^2 - 1)^2}{3\lambda^4 N} \tag{A.15}$$

Multiplying $R_{sca}(\lambda)$ by the distance travelled in the medium gives the quantity described in Equation 4.5. Since we are dealing with small collagen fibers rather than molecules of oxygen, we must determine the number of particles in the volume. According to Jacques [36], we can simulate Rayleigh scattering within the dermal layers using spheres (of radius $r$). Considering that 21% (by volume) of the dermis is composed of collagen fibers [36], we can compute the number of particles in the volume as:

$$N = \frac{0.21}{V_s} \tag{A.16}$$

where:

$V_s$ = volume of the sphere $\left(\frac{4}{3}\pi r^3\right)$.

If light is successfully scattered in a volume of collagen fibers, we need to compute the direction in which the light is scattered. Recall that the Rayleigh phase function can be seen as a probability density function which describes the probability of a wave being scattered in a particular direction. Hence, given random numbers uniformly distributed in the interval $[0..1]$, we can compute a direction of scattering using the perturbation angles given in Equation 4.4.

# Appendix B

# Trowbridge-Reitz Distribution Function

In this appendix, we present a description of the Trowbridge-Reitz distribution function used in the BioSpec model. This description should highlight the steps taken to go from the surface structure presentation by Trowbridge and Reitz to the distribution function used by the BioSpec model.

Recall the Trowbridge-Reitz surface structure function:

$$s_f = \frac{\sigma^4}{\left(\sigma^2 \cos^2 \alpha + \sin^2 \alpha\right)^2} \tag{B.1}$$

In order to derive a proper warping function from this surface structure function, we would need to first integrate the function, then invert and solve for $\alpha$. However, integrating the surface structure function in terms of $\alpha$ is difficult, and when we attempted this integration using Maple, the result was impractical. Thus, as an alternative, we chose to use the surface structure function itself as the distribution function. This task is easier, since all we should need to do is set the surface structure function equal to $\xi$, then solve for $\alpha$. However, for $\cos\alpha$ varying from 0 to 1, $s_f$ varies from $\sigma^4$ to 1, where as our uniformly distributed random number $\xi$ varies from 0 to 1. Hence, to obtain an angular warping function associated with the surface-structure function described above, we use the following approximation:

$$s_a = \sigma^4 - \sigma^4\xi + \xi \tag{B.2}$$

where:

$\xi$ = random number uniformly distributed in $[0, 1]$,

We then set our approximation equal to the original Trowbridge-Reitz surface structure function and solve for $\alpha$.

$$\sigma^4 - \sigma^4\xi + \xi = \frac{\sigma^4}{\left(\sigma^2 \cos^2\alpha + \sin^2\alpha\right)^2} \tag{B.3}$$

Taking the square root of both sides:

$$\left(\sigma^4 - \sigma^4\xi + \xi\right)^{\frac{1}{2}} = \frac{\sigma^2}{\sigma^2 \cos^2\alpha + \sin^2\alpha} \tag{B.4}$$

We now move the $\sigma^2$ to the left and substitute for the $\sin^2\alpha$:

$$\frac{\sigma^2}{\left(\sigma^4 - \sigma^4\xi + \xi\right)^{\frac{1}{2}}} = \sigma^2 \cos^2\alpha + \left(1 - \cos^2\alpha\right) \tag{B.5}$$

We reduce terms to get:

$$\frac{\sigma^2}{\left(\sigma^4 - \sigma^4\xi + \xi\right)^{\frac{1}{2}}} - 1 = \cos^2\alpha\left(\sigma^2 - 1\right) \tag{B.6}$$

Moving terms to the left we get:

$$\left(\frac{\sigma^2}{\left(\sigma^4 - \sigma^4\xi + \xi\right)^{\frac{1}{2}}} - 1\right)\frac{1}{\sigma^2 - 1} = \cos^2\alpha \tag{B.7}$$

And finally, solving for $\alpha$, we get:

$$\alpha = \arccos\left[\left(\left(\frac{\sigma^2}{\left(\sigma^4 - \sigma^4\xi + \xi\right)^{\frac{1}{2}}} - 1\right)\frac{1}{\sigma^2 - 1}\right)^{\frac{1}{2}}\right] \tag{B.8}$$

We realize the technique used here lacks a rigorous mathematical treatment, and is technically not a warping function derived from the original surface-structure function. However, the distribution function used by the BioSpec model, is based on and does use the original Trowbridge-Reitz function. Future experiments will attempt to quantify the impact of this approximation on accuracy. We also remark that it is possible to use a data driven mechanism (such as a table look-up) to compute the perturbation angle. Such a table look-up mechanism would have the benefit of being computationally faster (when compared to the distribution function used in BioSpec) and will use the original surface-structure function directly. However, the suitability of such a data driven approach needs to be examined in close detail and thus is future work.